



## 31 **Abstract**

32 Naturally competent bacteria encode sophisticated protein machineries for the uptake and  
33 translocation of exogenous DNA into the cell. If this DNA is integrated into the bacterial  
34 genome, the bacterium is said to be naturally transformed. Most competent bacterial species  
35 utilise type IV pili for the initial DNA uptake step. These proteinaceous cell-surface structures  
36 are composed of thousands of pilus subunits (pilins), designated as major or minor  
37 according to their relative abundance in the pilus. In this study, we show that the minor pilin  
38 FimT plays an important role in the natural transformation of *Legionella pneumophila*. We  
39 used NMR spectroscopy, *in vitro* DNA binding assays and *in vivo* transformation assays to  
40 understand the molecular basis of FimT's role in this process. FimT directly interacts with  
41 DNA *via* an electropositive patch, rich in arginines, several of which are well-conserved and  
42 located in FimT's conformationally flexible C-terminal tail. We also show that FimT  
43 orthologues from other  $\gamma$ -Proteobacteria share the ability to bind to DNA. Our functional  
44 characterisation and comprehensive bioinformatic analysis of FimT, suggest that it plays an  
45 important role for DNA uptake in a wide range of competent species.

46

## 47 **Introduction**

48 Competent bacteria can take up exogenous DNA, present in their environment, and  
49 integrate it into their genomes by the process of natural transformation. This is an important  
50 avenue of horizontal gene transfer (HGT), which has widespread consequences for bacterial  
51 evolution and the spread of antibiotic resistance and other pathogenicity traits. In contrast to  
52 other modes of HGT, namely transduction and conjugation, natural transformation is entirely  
53 controlled by the recipient cell that encodes all the required machinery for DNA uptake,  
54 translocation and integration<sup>1</sup>. More than 80 bacterial species, including Gram-negative and  
55 Gram-positive organisms, have been shown to be naturally competent<sup>2</sup>, yet the true  
56 prevalence of this mechanism amongst bacteria likely remains underappreciated. The Gram-  
57 negative bacterium *Legionella pneumophila* is naturally competent<sup>3</sup>, consistent with the  
58 observation that its genome bears evidence of frequent HGT and recombination events<sup>4-6</sup>.  
59 Although *L. pneumophila* could be described as an accidental human pathogen, it is the  
60 aetiological agent of Legionnaire's disease, a serious and life-threatening form of  
61 pneumonia, that results from an infection of alveolar macrophages by contaminated  
62 aerosols<sup>7,8</sup>.

63

64 *Legionella*, like most Gram-negative bacteria, are thought to utilise type IV pili (T4P) for DNA  
65 uptake<sup>3,9,10</sup>, defined as the movement of DNA across the outer membrane (OM) and into the  
66 periplasmic space<sup>11</sup>. However, the molecular mechanisms involved in this step remain poorly  
67 defined. T4P are extracellular proteinaceous appendages composed of thousands of

68 individual pilus subunits (pilins), designated as major or minor depending on their relative  
69 abundance in the pilus<sup>12,13</sup>. A prevailing model suggests that T4P can bind to DNA<sup>9</sup> and  
70 transport it into the cell *via* pilus retraction, which is powered by the retraction ATPase  
71 PilT<sup>14,15</sup>. Pilus retraction is thought to bring the DNA into proximity with the OM and be taken  
72 up across the OM-embedded secretin channel PilQ, which is the same pore traversed by the  
73 T4P themselves<sup>16,17</sup>. Once in the periplasm, ComEA binds to incoming DNA to prevent its  
74 back-diffusion by acting like a Brownian ratchet<sup>18,19</sup>. Subsequently, DNA is converted into  
75 single-stranded DNA (ssDNA) and transported across the inner membrane (IM) by a putative  
76 channel called ComEC<sup>20</sup>. In the cytoplasm, ssDNA is protected by single-stranded DNA  
77 binding protein (Ssb)<sup>21</sup> and DNA processing protein A (DprA)<sup>22</sup>, before being integrated into  
78 the genome by homologous recombination in a RecA- and ComM-dependent manner<sup>23,24</sup>.

79  
80 In recent years, studies of several competent bacteria have shown that their T4P (or their  
81 pilins) can directly interact with DNA<sup>15,25–29</sup>. This function was attributed to specialised minor  
82 pilins or pilin-like proteins in *Neisseria species* (ComP)<sup>27,28</sup>, *Vibrio cholerae* (VC0858 and  
83 VC0859)<sup>15</sup>, and *Thermus thermophilus* (ComZ)<sup>29</sup>, although a major pilin (PilA4) has also  
84 been suggested to contribute in the latter<sup>30</sup>. Of these, ComP found in *Neisseria* species, is  
85 the best-characterised DNA-binding minor pilin to date. ComP displays a sequence  
86 preference for neisserial DNA containing so-called DNA uptake sequences (DUS)<sup>31–33</sup> and  
87 binds to DNA through an electropositive surface patch<sup>27,28,34</sup>. VC0858, VC0859 and ComZ  
88 are thought to be located at the pilus tip<sup>15,29</sup>, whereas ComP has been suggested to either  
89 be incorporated throughout the pilus fibre<sup>28</sup> or at the pilus tip<sup>9</sup>. In addition to these proteins,  
90 the minor pilin FimT has also been implicated in natural transformation, as its loss leads to a  
91 reduction in transformation efficiency in *Acinetobacter bayly*<sup>35</sup>. However, this phenotype was  
92 never followed up with further DNA-binding studies.

93  
94 We set out to study DNA uptake during natural transformation in *Legionella pneumophila*. It  
95 is not known whether *Legionella*'s T4P can interact with DNA, and if so, which pilins are  
96 responsible. We tested several major and minor *Legionella* pilin candidates for their ability to  
97 bind DNA and show that FimT efficiently interacts with DNA *in vitro* and *in vivo*, and that loss  
98 of binding, just like *fimT* deletion, results in almost complete abrogation of natural  
99 transformation. We also determined the structure of FimT and show that a conserved  
100 electropositive surface patch rich in arginines is required for DNA binding. Finally, we show  
101 that FimT is not only important for natural transformation in *L. pneumophila*, but that it likely  
102 plays a role in many other bacterial species, as suggested by DNA binding studies and  
103 bioinformatic analyses. Together, our work provides the molecular basis of FimT's role in  
104 natural transformation.

## 105 Results

106

### 107 **FimT is critical for natural transformation in *L. pneumophila* and interacts with DNA**

108 FimT and FimU are minor type IV pilins that belong to the GspH/FimT family of proteins  
109 (Pfam: PF12019; InterPro: IPR022346), which also includes the type II secretion system  
110 (T2SS) pseudopilin GspH/XcpU. All three genes are encoded in the *L. pneumophila* genome  
111 and share an overall amino acid sequence identity of ~15–25%. *L. pneumophila* FimT  
112 (FimT<sub>Lp</sub>) and FimU (FimU<sub>Lp</sub>) possess all the features of typical type IV pilins, including an N-  
113 terminal signal sequence required for their targeting to the inner membrane (IM), followed by  
114 a hydrophobic transmembrane helix required for IM insertion prior to pilus assembly and  
115 proper packing into the filament structure post assembly<sup>12,36</sup>. First, we tested whether FimT<sub>Lp</sub>  
116 or FimU<sub>Lp</sub> are required for T4P biogenesis in *L. pneumophila*. To this end, we overexpressed  
117 a Flag-tagged version of the major pilin PilA2<sup>10</sup> and compared relative amounts of PilA2-  
118 Flag-containing T4P in fractions of surface appendages sheared from the cell surface of  
119 various *L. pneumophila* Lp02 strains, including *fimT* and *fimU* deletion strains (**Extended**  
120 **Data Fig. 1a**). These results indicate that T4P are still assembled and present on the cell  
121 surface when *fimT* or *fimU* are deleted. Next, to test whether FimT<sub>Lp</sub> or FimU<sub>Lp</sub> play a role in  
122 natural transformation in *L. pneumophila*, we performed transformation assays comparing  
123 the *fimT* and *fimU* deletion strains with the parental strain and strains harbouring deletions in  
124 genes known to be important for natural transformation (**Fig. 1a**). Deletion of *comEC*,  
125 encoding the putative IM DNA channel, *pilQ*, encoding the OM secretin, and *pilT*, encoding  
126 the retraction ATPase, resulted in undetectable levels of natural transformation in our assay.  
127 These observations are in close agreement with previous studies in *L. pneumophila*, as well  
128 as other competent Gram-negative organisms such as *V. cholerae*, where deletion of these  
129 genes resulted in severe or complete natural transformation phenotypes<sup>10,16</sup>. Deletion of  
130 *fimU* did not produce a phenotype, whereas natural transformation was undetectable in the  
131 *fimT* deletion strain, as observed previously in *A. bayly*<sup>35</sup>. Expression of FimT<sub>Lp</sub> *in trans* from  
132 an IPTG-inducible promoter restored the transformation efficiency of our *L. pneumophila*  
133 strain to wild-type levels, showing that the transformation defect is specific to FimT<sub>Lp</sub>.

134

135 We reasoned that FimT contributes to the OM DNA uptake step of natural transformation by  
136 forming a constituent part of type IV pili (T4P) able to directly bind to DNA. Therefore, we  
137 performed electrophoretic mobility shift assays (EMSA) to test whether FimT<sub>Lp</sub> is able to bind  
138 to DNA *in vitro* (**Fig. 1b**). In order to produce soluble protein samples, all pilins were  
139 expressed as truncations lacking the N-terminal transmembrane helix (**Extended Data**  
140 **Fig. 1b**). Indeed, purified FimT<sub>Lp</sub> interacted with all DNA probes tested (**Extended Data**  
141 **Table 4**), including ssDNA, dsDNA, linear and circular DNA molecules, whereas neither

142 FimU<sub>Lp</sub>, nor the putative major pilin subunits (PilA1 and PilA2) showed any interaction  
143 (**Fig. 1b** and **Extended Data Fig. 1c**). These experiments suggest that the dissociation  
144 constant ( $K_D$ ) of the interaction between FimT<sub>Lp</sub> and 30meric DNA is in the low  $\mu$ M range. In  
145 order to determine the  $K_D$  more precisely and to learn about the binding stoichiometry of this  
146 interaction, we performed isothermal titration calorimetry (ITC) utilising shorter 12meric  
147 ssDNA or dsDNA fragments (**Fig. 1c**). We determined a  $K_D$  of 7.0  $\mu$ M and 2.8  $\mu$ M for  
148 12meric ssDNA and dsDNA, respectively. Interestingly, these experiments revealed that a  
149 single FimT<sub>Lp</sub> binds to 12meric ssDNA, whereas two molecules can bind to the dsDNA  
150 ligand, suggesting two binding sites on opposite sides of the double helix.

151

### 152 **The solution structure of FimT<sub>Lp</sub>**

153 We determined the solution structure of the soluble N-terminally truncated (residues 28-152,  
154 mature pilin sequence numbering) FimT<sub>Lp</sub> by nuclear magnetic resonance (NMR)  
155 spectroscopy (**Fig. 2a**, **Table 1**). The structure consists of an N-terminal  $\alpha$ -helix ( $\alpha$ 1C) (the  
156 transmembrane portion of this helix,  $\alpha$ 1N, has been removed in the construct), two  $\beta$ -sheets  
157 that complete the C-terminal globular pilin domain, and a C-terminal tail, which exhibits  
158 conformational flexibility. Both  $\beta$ -sheets are composed of antiparallel strands:  $\beta$ -sheet I is  
159 formed by  $\beta$ 1,  $\beta$ 2,  $\beta$ 3 and  $\beta$ 5, and  $\beta$ -sheet II by  $\beta$ 4,  $\beta$ 6 and  $\beta$ 7. The closest structural  
160 homologue is FimU from *Pseudomonas aeruginosa* (FimU<sub>Pa</sub>) (PDB ID: 4IPU, 4IPV)  
161 (**Fig. 2b**). While the two structures share a common fold, there are some key differences. In  
162 the FimU<sub>Pa</sub> structure, the loop between  $\beta$ 2 and  $\beta$ 3 in  $\beta$ -sheet I forms an additional  $\beta$ -hairpin  
163 ( $\beta$ 2' and  $\beta$ 2''). It is possible, however, that this additional  $\beta$ -hairpin of FimU<sub>Pa</sub> simply  
164 represents the conformation captured in the crystal structure, as the length of the  $\beta$ 2- $\beta$ 3 loop  
165 is similar in both proteins. In addition, the  $\beta$ 7 strand of  $\beta$ -sheet II is longer in FimU<sub>Pa</sub> and it  
166 contains an additional strand ( $\beta$ 8)<sup>37</sup>. Furthermore, FimU<sub>Pa</sub> contains a disulphide bond  
167 connecting Cys127 of  $\beta$ 6 to the penultimate residue, Cys158, effectively stapling the  
168 C-terminal tail in place on top of  $\beta$ -sheet II. Such a disulphide bond is found in various major  
169 and minor pilins and the intervening sequence is known as the D-region<sup>36,38</sup>. Further  
170 structures of GspH/FimT family proteins exist, including of the minor T2SS pseudopilins,  
171 GspH from *Escherichia coli* (PDB ID: 2KNQ) and its orthologue EpsH from *V. cholerae* (PDB  
172 ID: 2QV8<sup>39</sup> and 4DQ9<sup>40</sup>), which display similar folds (**Extended Data Fig. 2**).

173

174 The C-terminal tail (residues 140–152) of FimT<sub>Lp</sub> is unique amongst the currently determined  
175 structures of GspH/FimT family members. Different pieces of NMR data suggest significant  
176 conformational exchange, but not an entirely flexibly disordered tail. The amide resonances  
177 of residues 140–149 are very weak and those of residues 142–144 are not visible at all. We  
178 could not observe any intense long-range nuclear Overhauser effects (NOEs) for residues

179 140–152, which would be expected for a well-defined  $\beta$ -sheet conformation.  $T_2$  relaxation  
180 measurements indicated conformational exchange on the millisecond timescale, as the  $T_2$   
181 values for backbone amide  $^1\text{H}$  and  $^{15}\text{N}$  nuclei for the C-terminal tail were approximately half  
182 the value of the structured part of the protein (**Fig. 2d, Extended Data Fig. 3**). A fully  
183 disordered C-terminal tail could however be excluded by  $\{^1\text{H}\}$ - $^{15}\text{N}$  heteronuclear NOE  
184 measurements, as the NOE intensity for the amides in the tail was close to the theoretical  
185 value of 0.78, which is expected for amides on globular particles. Finally, the deviations of  
186  $\text{C}\alpha$  chemical shifts from random coil values clearly indicated a  $\beta$ -strand propensity (**Fig. 2d,**  
187 **Extended Data Fig. 3**). The data therefore suggest that the C-terminal amino acids have a  
188  $\beta$ -strand-like backbone conformation but sample different states in the micro- to millisecond  
189 timescale. These findings are further supported by low amide proton temperature  
190 coefficients<sup>41</sup> and increased proteolytic susceptibility of this region, compared to the rest of  
191 the structure, witnessed by disappearance of the NMR resonances of the tail after prolonged  
192 storage of samples.

193

#### 194 **FimT<sub>Lp</sub> interacts with DNA via a conserved C-terminal region rich in arginines**

195 Next, we characterised the residues of FimT<sub>Lp</sub> involved in DNA binding using NMR  
196 spectroscopy (**Fig. 3a-c**). We performed binding experiments titrating increasing amounts of  
197 12 bp dsDNA (**Extended Data Table 4**) into  $^{15}\text{N}$ -labelled FimT<sub>Lp</sub> and recorded  $^{15}\text{N}$ ,  $^1\text{H}$   
198 heteronuclear single-quantum correlation (2D [ $^{15}\text{N}$ ,  $^1\text{H}$ ]-HSQC) spectra. Most FimT<sub>Lp</sub>  
199 resonances remained unperturbed (**Fig. 3a**), which suggests that no global conformational  
200 change occurs upon DNA binding. However, a subset of resonances exhibit marked  
201 chemical shift perturbations (CSPs) (**Fig. 3a**), indicating changes in the local chemical  
202 environment resulting from direct contact with DNA or other indirect conformational changes.  
203 A plot of CSPs against the amino acid sequence is shown in **Figure 3b**, and we mapped  
204 CSPs greater than a threshold ( $\Delta\text{ppm} > 1\sigma$ ) onto the FimT<sub>Lp</sub> surface (**Fig. 3c, Extended**  
205 **Data Fig. 4**). The largest CSPs correspond to residues located in three adjacent loop  
206 regions in the C-terminal globular domain of the protein, the  $\beta 4$ - $\beta 5$  loop (residues 103–106),  
207 the  $\beta 5$ - $\beta 6$  loop (118–126) and the C-terminal tail (140–152) (**Fig. 3b**). These shifts  
208 predominantly map to an elongated surface patch connecting the C-terminal tail with the  
209 globular C-terminal domain of FimT<sub>Lp</sub> (**Fig. 3c**). Most of these residues are predicted to be  
210 accessible in the context of the assembled pilus, particularly when considering the flexibility  
211 of this region (**Fig. 2d, Extended Data Fig. 3**). CSPs corresponding to residues outside this  
212 contiguous surface patch can be explained by indirect conformational changes. We  
213 attempted to further structurally characterise the DNA-bound state, with special emphasis on  
214 possible changes in the structure or dynamics of the C-terminus. However, the FimT<sub>Lp</sub>-DNA  
215 complex was not stable long-term and NMR signals were generally strongly weakened upon

216 DNA binding, such that relaxation or triple resonance experiments did not yield spectra of  
217 sufficient quality. An analysis of evolutionary conservation of the FimT<sub>Lp</sub> surface revealed  
218 that many of the interacting residues are also well conserved (**Fig. 3c**). In particular,  
219 residues of the C-terminal tail show marked sequence conservation and include a number of  
220 positively charged arginines, which are often involved in protein-DNA contacts through  
221 binding to the negatively charged DNA backbone *via* electrostatic interactions<sup>42</sup>.

222

### 223 **Interface mutations inhibit DNA binding and natural transformation *in vivo***

224 We conducted microscale thermophoresis/temperature-related intensity change (MST/TRIC)  
225 experiments to measure the binding of labelled 12 bp dsDNA (**Extended Data Table 4**) to  
226 purified FimT<sub>Lp</sub> variants (**Extended Data Fig. 1b**), in order to further understand the nature  
227 of the FimT<sub>Lp</sub>-DNA interaction and the importance of specific interface residues. First, we  
228 conducted experiments under different buffer conditions to test whether the affinity of the  
229 interaction between wild-type FimT<sub>Lp</sub> and DNA is dependent on ionic strength. Indeed, when  
230 we increased the NaCl concentration from 50 mM to 150 mM, thereby raising the ionic  
231 strength, the  $K_D$  increased from ~6.3  $\mu$ M to ~70.1  $\mu$ M (**Fig. 4a**). This is consistent with a non-  
232 sequence specific protein-DNA interaction, which is electrostatically driven. Furthermore, the  
233  $K_D$  determined at a NaCl concentration of 50 mM agrees very well with the affinities  
234 determined from the ITC experiments ( $K_D$  of 2.8  $\mu$ M) (**Fig. 1c**), as well as our NMR binding  
235 studies ( $K_D$  of ~8  $\mu$ M) (**Extended Data Fig. 5**), which were all conducted in the same buffer.  
236 Next, we used MST/TRIC to test the importance of several charged residues at the DNA  
237 binding interface identified by our NMR analyses (**Fig. 4b**). We substituted arginine or lysine  
238 residues for glutamine in the three loop regions we identified to be important for binding. As  
239 expected, the loss of a single charged residue (e.g. K103 in the  $\beta$ 4- $\beta$ 5 loop; R119 in the  
240  $\beta$ 5- $\beta$ 6 loop; R143, R146 or R148 in the C-terminal tail) only led to a small reduction in the  
241 affinity (~1.4–4 fold). However, the combined loss of two (R146/R148) or three  
242 (R143/R146/R148) charged residues next to each other on the FimT<sub>Lp</sub> surface was more  
243 detrimental to binding, resulting in a ~10 fold or ~45 fold reduction in affinity, respectively.  
244 Lastly, we tested what effect these binding mutations have on natural transformation *in vivo*  
245 (**Fig. 4c**). These data show that mutations of single charged residues reduce *Legionella*'s  
246 transformability by ~30-600 fold, whereas the double and triple mutants completely abrogate  
247 DNA uptake in our assay and thus phenocopy the effect observed upon *fimT* deletion  
248 (**Fig. 1a**). These results further support a model in which FimT<sub>Lp</sub> contributes to natural  
249 transformation in *Legionella* by virtue of its ability to interact with DNA in the context of a  
250 DNA uptake pilus.

251

252

## 253 **FimT of other Gram-negative bacteria also interacts with DNA**

254 Given that FimT, and the residues involved in DNA binding identified in FimT<sub>Lp</sub>, appear to be  
255 conserved, we wondered whether FimT orthologues from other bacteria are also capable of  
256 binding DNA. We expressed and purified FimT and FimU from the human pathogen  
257 *P. aeruginosa* and the plant pathogen *Xanthomonas campestris* (both  $\gamma$ -Proteobacteria) and  
258 performed EMSAs to assess DNA binding *in vitro* (**Fig. 5a**). Interestingly, FimT from both  
259 species binds to DNA and the affinity appears to be within the same order of magnitude as  
260 *L. pneumophila* FimT. On the other hand, FimU does not interact with DNA, except for the  
261 *X. campestris* homologue, which shows very weak binding at very high FimU concentrations.  
262 Since both FimT orthologues (FimT<sub>Pa</sub> and FimT<sub>Xc</sub>) likely share structural similarities to  
263 FimT<sub>Lp</sub>, we tested whether they are capable of restoring natural transformability in a  
264 *L. pneumophila fimT* deletion strain. The FimT orthologues were ectopically expressed either  
265 as wild-type full-length proteins or as chimeric proteins. The chimeric constructs replaced the  
266 flexible C-terminal tail region (lacking a disulphide bond) of FimT<sub>Lp</sub> with the *bona fide*  
267 D-region of the FimT orthologues (**Fig. 5b**). The expression of full-length FimT<sub>Pa</sub> and FimT<sub>Xc</sub>  
268 did not restore natural transformation. Intriguingly, when we replaced the flexible C-terminal  
269 tail of FimT<sub>Lp</sub> with the D-region of FimT<sub>Pa</sub>, natural transformation levels were restored to near  
270 wild-type levels. Together, these results indicate that DNA binding by FimT is not unique to  
271 *L. pneumophila* and that FimT may be important for DNA uptake in a wide range of  
272 competent species.

273  
274 We then used genomic context and sequence information from the four FimT orthologs  
275 known to either bind to DNA or contribute to competence (from *L. pneumophila*,  
276 *X. campestris*, *P. aeruginosa* and *A. baylyi*) to explore the distribution and conservation of  
277 this protein (see Methods). First, we looked at the genetic location and organisation of FimT  
278 and FimU in *Legionella* and other bacteria (**Extended Data Fig. 6**). In *L. pneumophila*, *fimU*  
279 (*lpg0632*) is encoded in a minor pilin operon upstream of *pilV* (*lpg0631*), *pilW* (*lpg0630*), *pilX*  
280 (*lpg0629*), *pilY1* (*lpg0628*) and *pilE* (*lpg0627*). In contrast, *fimT* (*lpg1428*) appears as an  
281 'orphan' gene, encoded elsewhere in the genome, and seemingly distant from genes  
282 encoding other type IV pilins, components of the T4P machinery or genes with known  
283 functions in natural transformation. Interestingly, while FimT in other species could be found  
284 either as an orphan, or adjacent to other minor pilin-related genes, the location of FimU was  
285 conserved, and this pattern was seen in a broader collection of homologues as well as the  
286 functionally-characterised representatives. We then retrieved a diverse set of homologues of  
287 FimT<sub>Lp</sub> and classified them according to genomic location and sequence similarity to exclude  
288 sequences that were likely to be FimU proteins. We found that FimT is conserved in all  
289 sequenced *Legionella* species, and homologues are found in a wide variety of



290  $\gamma$ -Proteobacteria from various phylogenetic orders, with representatives of the  
291 Xanthomonadales, Alteromonadales and Pseudomonadales being particularly common  
292 (**Fig. 5c**). The pairwise sequence identity was 40-50% between FimTs from *Legionella*  
293 *pneumophila* and other *Legionella* species, and ~25% (median) between *L. pneumophila*  
294 FimT and those from more distantly related bacteria. Around half of the FimT homologues  
295 are located in proximity (within 5 kb) to other minor pilin locus components. FimU is also  
296 present in many bacterial species, albeit not all species encode both genes. Phylogenetic  
297 analysis of FimT homologues showed that these proteins largely clustered with others from  
298 the same order and sharing the same locus type, indicating that *fimT* is likely to be vertically  
299 inherited. The best conserved regions of FimT include the N-terminal helix, important for  
300 pilus biogenesis (IM insertion, assembly and structural packing), and the C-terminal region  
301 (**Fig. 5d**). This region of conservation includes many of the residues we have identified to be  
302 important for DNA binding and thus natural transformation (**Fig. 3c, d**). Indeed, it appears as  
303 though these DNA binding residues can be identified in proteins with as little as 18% overall  
304 amino acid sequence identity with FimT<sub>Lp</sub>. Taken together, FimT homologues share an  
305 overall fold and a conserved DNA-binding motif near the C-terminus of the protein, and can  
306 be found in diverse genomic locations within diverse proteobacterial species.

307

## 308 **Discussion**

309 Natural transformation is an important mode of horizontal gene transfer with widespread  
310 consequences for bacterial evolution. Furthermore, the spread of pathogenicity traits and  
311 antibiotic resistance genes leads to the emergence of increasingly virulent and difficult to  
312 treat bacterial strains. The first step of this process involves DNA uptake mediated by T4P<sup>9</sup>,  
313 which has only been studied in a handful of competent species. The minor type IV pilin  
314 FimT, but not the closely related FimU, from *A. baylyi* was previously implicated in natural  
315 transformation<sup>35</sup>, yet its mechanism remained obscure. Here, we characterised FimT from  
316 the naturally competent human pathogen *L. pneumophila* (FimT<sub>Lp</sub>) and revealed the  
317 molecular mechanisms underlying its role in natural transformation.

318

319 We hypothesised that FimT<sub>Lp</sub> is involved in DNA uptake by binding to extracellular DNA in  
320 the context of T4P and showed that *Legionella* strains lacking *fimT* display a marked  
321 reduction in transformation efficiency (**Fig. 1a**). Indeed, purified FimT<sub>Lp</sub> interacted with DNA  
322 *in vitro*, regardless of the nature of DNA probe tested (**Fig. 1b, Extended Data Fig. 1c**).  
323 Furthermore, we determined the structure of FimT<sub>Lp</sub> by NMR spectroscopy (**Fig. 2**) and  
324 mapped its DNA interaction surface by chemical shift perturbation experiments (**Fig. 3**). This  
325 binding surface consists of several positively charged residues, some of which are highly  
326 conserved, located primarily in two loop regions (the  $\beta$ 4- $\beta$ 5 and  $\beta$ 5- $\beta$ 6 loops) and the

327 C-terminal tail (**Fig. 3b, c**). The importance of key residues for DNA binding and natural  
328 transformation was confirmed by *in vitro* DNA binding assays and *in vivo* transformation  
329 assays (**Fig. 4b, c**). Although our ITC experiments (**Fig. 1c**) indicate a 2:1 (FimT<sub>Lp</sub>:DNA)  
330 binding mode, we do not think this is physiologically relevant in the context of the T4P.

331  
332 Our structure of FimT<sub>Lp</sub> shares the same overall fold as the closely related T4P minor pilin  
333 FimU<sub>Pa</sub>, and the T2SS minor pseudopilins GspH<sub>Ec</sub> and EpsH<sub>Vc</sub>, albeit with some key  
334 differences (**Fig. 2, Extended Data Fig. 2**). In place of the last  $\beta$ -strand ( $\beta 8$ ), part of  $\beta$ -sheet  
335 II in all other currently determined FimT/GspH family structures, FimT<sub>Lp</sub> contains a  
336 conformationally flexible C-terminal tail (**Extended Data Fig. 3**). In our NMR studies, the  
337 heteronuclear  $\{^1\text{H}\}$ - $^{15}\text{N}$  NOE data and C $\alpha$  chemical shifts for the C-terminal residues are  
338 indicative of a  $\beta$ -strand conformation, while the T<sub>2</sub> transverse relaxation times for backbone  
339 amide  $^1\text{H}$  and  $^{15}\text{N}$  nuclei, increased line broadening and the absence of H-bonds indicate a  
340 less well-structured conformation. A plausible interpretation of these results is that this  
341 region can exchange between a  $\beta$ -strand and a less-structured conformation on a  
342 millisecond timescale. The flexibility of this region is further supported by its increased  
343 proteolytic susceptibility. FimT<sub>Lp</sub>, as well as all FimT homologues from the order  
344 Legionellales, lack the D-region defining disulphide bond present in many major and minor  
345 pilins, including other FimT and FimU homologues (**Fig. 5d**). Therefore, it is likely that  
346 disulphide bond-containing FimT orthologues do not possess a conformationally flexible  
347 C-terminal tail. The structure of GspH<sub>Ec</sub> was also determined in solution by NMR  
348 spectroscopy, yet it possesses a clearly defined and complete four-stranded  $\beta$ -sheet II  
349 region. This suggests that this region, also shared by FimU<sub>Pa</sub> and EpsH<sub>Vc</sub>, is not simply a  
350 result of crystal lattice effects and thus further highlights FimT<sub>Lp</sub>'s unique C-terminal tail  
351 (**Fig. 2, Extended Data Fig. 2**).

352  
353 FimU and GspH/EpsH have been suggested to serve as adaptors in T4P and T2SS  
354 pseudopili, respectively, linking the tip subunits to the remainder of the filament structure  
355 composed of the major pilin subunit<sup>43–45</sup>. Whereas minor pilins in general have been  
356 suggested to play a role in pilus priming/pilus biogenesis<sup>37,45</sup>, the deletion of FimU, but not  
357 FimT affected pilus biogenesis in *P. aeruginosa* and *Pseudomonas syringae*<sup>46,47</sup>.  
358 Furthermore, FimU, but not FimT of *P. aeruginosa* has been shown to play a role in bacterial  
359 twitching motility<sup>48</sup>. In *A. baylyi* on the other hand, both proteins showed near wild-type levels  
360 of twitching, but FimT appeared to play a role in natural transformation<sup>35</sup>. Orthologues of the  
361 GspH pseudopilin are critical components of the T2SS and may play a role in binding to  
362 T2SS protein substrates<sup>49</sup>. To this end, the crystal structure of the *V. cholerae* orthologue  
363 EpsH revealed an extended and disordered  $\beta 4$ - $\beta 5$  loop (**Extended Data Fig. 2d**), which has

364 been proposed to play a role in substrate binding<sup>40</sup>. Interestingly, we have identified this  
365 same loop to contribute to FimT<sub>Lp</sub>-DNA binding (**Fig. 3b**). Therefore it appears that, although  
366 sharing a common evolutionary origin<sup>50</sup>, FimT/GspH family proteins have become  
367 functionally diverged and specialised for the binding of different macromolecular  
368 substrates<sup>51,52</sup>. In the case of FimT<sub>Lp</sub>, a surface patch rich in arginines enables it to function  
369 in DNA uptake during natural transformation.

370

371 The currently best-characterised DNA binding minor pilin is ComP<sup>27,28,34</sup>. While ComP  
372 homologues seem to be restricted to species of the family *Neisseriaceae*<sup>27</sup>, FimT  
373 homologues are present in diverse  $\gamma$ -Proteobacteria and some Hydrophilales (**Fig. 5c**). Both  
374 proteins share a conserved type IV pilin core structure, including the N-terminal helix and a  
375 four-stranded antiparallel  $\beta$ -sheet, but differ substantially in their C-terminal regions. In the  
376 case of ComP, this region is characterised by its so-called DD-region containing two  
377 disulphide bonds<sup>27</sup> (**Extended Data Fig. 7**). By contrast, FimT contains a second three-  
378 stranded antiparallel  $\beta$ -sheet followed by its conformationally flexible C-terminal tail and  
379 contains no disulphide bonds. In both proteins, important DNA binding residues are located  
380 near the C-terminus, which would be exposed to the solvent in the context of a fully  
381 assembled pilus<sup>28</sup>. Interestingly, competent *Neisseriaceae* species preferentially take up  
382 DNA sequences from related species<sup>31-33</sup>. This has been attributed to ComP's increased  
383 binding affinity towards DUS-sequences, which are DNA sequences that are highly enriched  
384 in their own genomes<sup>27</sup>. It was proposed that ComP engages DNA *via* an initial electrostatic  
385 attraction, followed by ComP's  $\alpha 1$ - $\beta 1$ ,  $\beta 1$ - $\beta 2$ , DD-region binding to successive grooves of the  
386 dsDNA to achieve specificity<sup>28</sup>. In contrast, no sequence selectivity has been reported for  
387 *L. pneumophila*<sup>3</sup>, which is consistent with the electrostatic binding mode of FimT<sub>Lp</sub>. In  
388 addition to FimT<sub>Lp</sub> and ComP, other type IV pilins or pilin-like proteins that contribute to T4P  
389 DNA binding include ComZ and Pila4 from *T. thermophilus*<sup>29,30</sup> and VC0858 and VC0859  
390 from *V. cholerae*<sup>15</sup>. Once again, positively charged lysine and/or arginine residues likely  
391 contribute to DNA binding in all these proteins.

392

393 Lastly, we showed that other FimT orthologues, including FimT of the human pathogen  
394 *P. aeruginosa* and the plant pathogen *X. campestris*, are also capable of DNA binding  
395 (**Fig. 5a**). These experiments showed that FimT orthologues, whether they contain or lack  
396 the D-region defining disulphide bond, are capable of DNA binding. This was demonstrated  
397 even more strikingly by the FimT chimera, where the fusion of FimT<sub>Lp</sub> with FimT<sub>Pa</sub> introduced  
398 a non-native disulphide bond into the *Legionella* system, yet resulted in a functional protein  
399 *in vivo* capable of supporting natural transformation (**Fig. 5b**). In addition, our bioinformatic

400 analyses showed that FimT is present across a wide range of  $\gamma$ -Proteobacteria and that the  
401 DNA-binding C-terminal region is well-conserved on a sequence level (**Fig. 5d**). In particular,  
402 our alignments of high-confidence FimTs revealed a conserved GRxR motif (where x is  
403 often, but not always, a hydrophobic residue) at their C-terminus (**Fig. 5d**). In FimT<sub>Lp</sub> these  
404 two arginines correspond to R146 and R148, which we showed contribute to DNA binding *in*  
405 *vitro* and *in vivo* (**Fig. 4b, c**). This motif is less well defined or only partially present in FimU  
406 orthologues and those we tested in this study do not bind DNA *in vitro* (**Fig. 5a**).  
407 Interestingly, a similar C-terminal motif can also be found in the pilins that assemble into the  
408 Com pili of Gram-positive organisms, which have been implicated in DNA uptake during  
409 natural transformation<sup>53–55</sup>. It remains to be investigated, whether this motif also contributes  
410 to DNA binding and natural transformation in those proteins.

411  
412 In summary, this study provides a comprehensive analysis of the molecular mechanisms  
413 underpinning FimT's interaction with DNA and demonstrated its pivotal role during natural  
414 transformation of the human pathogen *L. pneumophila*. Furthermore, we analysed FimT  
415 orthologues from other naturally competent and pathogenic  $\gamma$ -Proteobacteria, which together  
416 with our thorough bioinformatic analysis, suggests that FimT is a key player in the natural  
417 transformation of a wide range of bacteria.

418  
419  
420  
421  
422  
423  
424  
425  
426  
427  
428  
429  
430  
431  
432  
433  
434  
435

## 436 **Methods**

437

### 438 **Bacterial strains and growth conditions**

439 *L. pneumophila* Lp02 (laboratory strain derived from *L. pneumophila* Philadelphia-1) was  
440 cultured in ACES [N-(2-acetamido)-2-aminoethanesulfonic acid]-buffered yeast extract  
441 (AYE) liquid medium or on ACES-buffered charcoal yeast extract (CYE) solid medium,  
442 supplemented with 100 µg/mL streptomycin and 100 µg/mL thymidine. When appropriate,  
443 chloramphenicol and kanamycin were added at 5 µg/mL and 15 µg/mL, respectively. For the  
444 construction of knockout Lp02 strains, the relevant genes and 1000 bp of upstream and  
445 downstream regions were first cloned into the pSR47S suicide plasmid (derivative of  
446 pSR47<sup>56</sup>). Following deletion of the gene of interest from the plasmid, the modification was  
447 introduced onto the Lp02 chromosome by triparental conjugation and subsequent selection  
448 as described previously<sup>57,58</sup>. All strains were verified by colony PCR and DNA sequencing  
449 (Microsynth) and are listed in **Extended Data Table 2**.

450

### 451 **Plasmids**

452 All protein expression constructs were generated using the pOPINS or pOPINB vectors<sup>59,60</sup>  
453 carrying an N-terminal His<sub>6</sub>-SUMO or His<sub>6</sub> tag, respectively. Constructs for *in vivo* studies  
454 were generated using pMMB207C<sup>61</sup>, by cloning the relevant genes downstream of the *Ptac*  
455 promoter. DNA fragments were amplified from *L. pneumophila* (RefSeq NC\_002942.5)  
456 genomic DNA by PCR using CloneAmp HiFi PCR premix (Takara) and the relevant primers.  
457 For FimT and FimU orthologues from *P. aeruginosa* PAO1 (RefSeq NC\_002516.2) and  
458 *X. campestris pv. campestris* str. ATCC 33913 (RefSeq NC\_003902.1), template DNA was  
459 first synthesised (Twist Bioscience). In-Fusion cloning and site-directed mutagenesis was  
460 carried out according to the manufacturer's guidelines (Takara). All plasmids and primers  
461 used in this study can be found in **Extended Data Table 3** and **Extended Data Table 4**,  
462 respectively. A summary of the gene locus tags of genes mentioned in this study from their  
463 respective genomes can be found in **Extended Data Table 5** and **Extended Data Table 6**.

464

### 465 **Protein Production**

466 Recombinant His<sub>6</sub>-SUMO tagged proteins (FimT<sub>Lp</sub>, FimU<sub>Lp</sub>, FimT<sub>Pa</sub>, FimU<sub>Pa</sub>, FimT<sub>Xc</sub>, FimU<sub>Xc</sub>)  
467 and His<sub>6</sub>-tagged proteins (PilA1, PilA2) were expressed in BL21 (DE3) or Shuffle T7 *E. coli*  
468 cells (NEB). All constructs were N-terminally truncated to remove the transmembrane helix  
469 ( $\alpha$ 1N) (**Extended Data Table 3**). Cultures were grown in Luria-Bertani (LB) media to an  
470 optical density at 600 nm (OD<sub>600</sub>) of 0.6–0.8, induced using 0.5 mM IPTG and further  
471 incubated at 16°C for 12–18 h while shaking. Cells were lysed in 50 mM Tris-HCl pH 7.2, 1  
472 M NaCl, 20 mM imidazole, 0.1 mg/mL lysozyme, 1 mg/mL DNase and one complete mini

473 EDTA-free protease inhibitor cocktail tablet (Roche), by passing the sample three times  
474 through a pressurised cell disruptor (M110-L, Microfluidics) at 12000 psi. The clarified lysate  
475 was applied to a 5 mL HisTrap HP column (Cytiva) and His<sub>6</sub>-SUMO or His<sub>6</sub> tagged pilins  
476 were eluted with a linear 20–500 mM imidazole gradient. The His<sub>6</sub>-SUMO or His<sub>6</sub> tag was  
477 cleaved using the catalytic domain of the human SENP1 protease or PreScission protease,  
478 respectively, while the sample was dialysed against 50 mM Tris-HCl pH 7.2, 50 mM NaCl.  
479 Protein samples were further purified by cation exchange chromatography using a 5 mL  
480 HiTrap SP HP column (Cytiva), from which pilins were eluted using a linear 50–1000 mM  
481 NaCl gradient. Lastly, the pilin samples were purified by size exclusion chromatography in  
482 50 mM Tris-HCl pH 7.2, 50 mM NaCl using a HiLoad 16/600 Superdex 75 pg column  
483 (Cytiva). Protein samples were concentrated using Amicon Ultra-15 centrifugal filters (3 kDa  
484 molecular weight cut-off, Millipore). Reducing agent (2 mM DTT) was included in the buffers  
485 for those pilins with free cysteines. All purification steps were performed at 4°C.

486

## 487 **NMR spectroscopy**

### 488 *Production of isotope-labelled FimT<sub>Lp</sub>*

489 To produce uniformly labelled FimT<sub>Lp</sub>, cells were grown in M9 minimal medium containing  
490 1 g/L <sup>15</sup>NH<sub>4</sub>Cl and further supplemented with 3 g/L glucose (or <sup>13</sup>C<sub>6</sub>-glucose for double  
491 labelled FimT<sub>Lp</sub>), 2 mM MgSO<sub>4</sub>, trace elements, vitamin mix and appropriate antibiotics for  
492 selection. Protein expression was induced at an OD<sub>600</sub> of 0.6–0.8 with 0.5 mM IPTG and  
493 cells were harvested after 20 h at 16°C. FimT<sub>Lp</sub> was purified as described above.

494

### 495 *Data acquisition and structure determination*

496 For resonance assignments and structure determination the following spectra were recorded  
497 on a 580 μM sample of (u-<sup>13</sup>C,<sup>15</sup>N)-labeled FimT 28–152 in 25 mM NaP<sub>i</sub> pH 7.2, 150 mM  
498 NaCl and 10% D<sub>2</sub>O at 298 K in a 3 mm diameter NMR tube: 3D HNCACB and 3D  
499 CBCACONH spectra<sup>62</sup> were recorded on a 700 MHz AVIIIHD spectrometer equipped with a  
500 TCI cryoprobe (Bruker). The spectra consisted of 2048×50×100 complex points in the <sup>1</sup>H,  
501 <sup>15</sup>N and <sup>13</sup>C dimensions with respective spectral widths of 16, 34 and 64 ppm, and were  
502 recorded with 8 scans per increment resulting in 2 and 1.5 days of measurement time,  
503 respectively. A 3D HcC(alia)H-TOCSY<sup>63</sup> was recorded on a 600 MHz AVIIIHD  
504 spectrometer equipped with a TCI cryoprobe (Bruker). The spectrum consisted of  
505 1536×100×150 complex points in the <sup>1</sup>H, <sup>1</sup>H and <sup>13</sup>C dimensions with respective spectral  
506 widths of 16, 12 and 140 ppm and was recorded with 2 scans per increment in 3 days using  
507 a recycle delay of 2 s. A time shared 3D [<sup>13</sup>C/<sup>15</sup>N,<sup>1</sup>H]-HSQC NOESY (modified from<sup>64</sup>) was  
508 recorded on a 900 MHz AVIIIHD spectrometer equipped with a TCI cryoprobe (Bruker). The  
509 spectrum consisted of 1536×100×256 complex points in the <sup>1</sup>H, <sup>1</sup>H and <sup>13</sup>C/<sup>15</sup>N dimensions

510 with respective spectral widths of 16, 12 and 140/58 ppm and was recorded with 2 scans per  
511 increment in 3 days.

512

513 Resonance assignments were determined with the program cara ([www.cara.nmr.ch](http://www.cara.nmr.ch), Keller

514 R (2005), ETH Zürich) to 98.2% completeness. Signals in the NOESY spectra were

515 subsequently automatically picked in the program analysis of the ccpnmr 2.5.1 software

516 package<sup>65</sup>. Peaklists and assignments were used as input for a structure calculation with

517 cyana<sup>66</sup> where angle constraints were automatically generated from C $\alpha$  chemical shifts.

518 Manual inspection of the automatically picked peak lists resulted in a set of 4595 picked

519 NOE peaks of which 4220 were assigned in the final cyana calculation which yielded an

520 average target function value of 0.21. The structures were finally energy minimized in the

521 program amber20<sup>67</sup>. Statistics for the resulting bundle of 20 conformers can be found in

522 **Table 1**. Additional analysis of the structural bundle after the cyana calculation revealed 42

523 hydrogen bonds (each present in more than 6 structures) and the following Ramachandran

524 statistics: 72.2%, 27.4% and 0.4% of residues in favoured, allowed and additionally allowed

525 regions, respectively. All structural figures were generated using PyMOL

526 (<https://www.pymol.org>).

527

#### 528 *DNA binding studies by NMR*

529 To map the surface patch of FimT<sub>Lp</sub> involved in DNA binding, chemical shift perturbation

530 experiments were performed using 12 bp or 36 bp dsDNA fragments (**Extended Data**

531 **Table 4**). [<sup>15</sup>N,<sup>1</sup>H]-HSQC experiments of 80  $\mu$ M <sup>15</sup>N-labelled FimT<sub>Lp</sub> at saturating

532 concentrations of DNA were recorded. In order to use the same conditions as other assays,

533 all protein and DNA samples for NMR binding studies were dialysed into 50 mM Tris-HCl

534 pH 7.2, 50 mM NaCl buffer. Weighted chemical shift perturbations (CSPs), defined as

535  $((\Delta^1\text{H}^2)^{0.5} + ((\Delta^{15}\text{N}/5)^2)^{0.5}$  (ppm), were measured by comparing spectra of unbound and bound

536 states. The standard deviation ( $\sigma$ ) of the chemical shift range was calculated, CSP maps

537 were plotted in GraphPad Prism v9 and residues for which the shift change was greater than

538  $\sigma$  were mapped onto the FimT<sub>Lp</sub> surface. To estimate the equilibrium dissociation constant

539 ( $K_D$ ) of this interaction, [<sup>15</sup>N,<sup>1</sup>H]-HSQC experiments of 40  $\mu$ M <sup>15</sup>N-labelled FimT<sub>Lp</sub> at different

540 concentrations (0–600  $\mu$ M) of DNA were recorded. For selected residues undergoing large

541 CSPs, binding curves were plotted and fitted to a model assuming one set of binding sites

542 using the software fitKD (four representative curves are shown in (**Extended data Fig. 5**)).

543 The spectra were recorded on a 700 MHz AV-NEO spectrometer equipped with a TCI

544 cryoprobe (Bruker) and consisted of 2048 $\times$ 128 complex points using 32 scans per increment

545 resulting in an experiment time of 2 h.

546

## 547 **Electrophoretic mobility shift assay**

548 Various DNA probes were tested for interaction with purified pilin samples using an agarose  
549 gel-based electrophoretic mobility shift assay (EMSA). Short 30 bp dsDNA fragments were  
550 generated by annealing complementary strands of the appropriate length. To generate  
551 fluorescently labelled dsDNA probes, one of the two annealing strands was labelled at the  
552 5' end with fluorescein (FAM). All oligonucleotides were obtained from Microsynth and are  
553 listed in **Extended Data Table 4**. The pTRC99A-*lpg2953-2958::Kan* (9074 bp) plasmid, left  
554 intact or linearised by a single-cutter restriction enzyme (ClaI), was used for the comparison  
555 between circular and linear dsDNA probes, respectively. All DNA probes were resuspended  
556 in or dialysed into the same buffer as the protein samples prior to the assay. DNA samples  
557 (1  $\mu$ M of 30-meric ssDNA and dsDNA; 20 ng/ $\mu$ l for longer DNA fragments) were incubated  
558 with increasing concentrations (0-100  $\mu$ M) of pilins in 50 mM Tris-HCl pH 7.2, 50 mM NaCl,  
559 15% (v/v) glycerol in a final volume of 20  $\mu$ L. These samples were incubated at 25°C for  
560 30 min and subsequently separated by gel electrophoresis at 10 V/cm for 30 min using 0.9-  
561 2.5% (w/v) agarose gels containing SYBR Safe DNA stain (Invitrogen). DNA was visualised  
562 using UV illumination in a gel imaging system (Carestream).

563

## 564 **Isothermal Titration Calorimetry**

565 Isothermal titration calorimetry (ITC) experiments were carried out in duplicate on a VP-ITC  
566 microcalorimeter (MicroCal). All measurements were performed in 50 mM Tris-HCl pH 7.2,  
567 50 mM NaCl buffer at 30°C. Following a pre-injection of 1  $\mu$ L, titrations consisted of 19  
568 consecutive 15  $\mu$ L injections of 320  $\mu$ M 12meric dsDNA or 350  $\mu$ M ssDNA (syringe) into  
569 30  $\mu$ M FimT<sub>Lp</sub> (cell) performed at 180 s or 240 s intervals, respectively. The heat of ligand  
570 dilution, obtained by injecting DNA into buffer, was subtracted from the reaction heat, and  
571 curve fitting was performed in Origin (OriginLab) using a model assuming two binding sites  
572 of equal affinity or “one set” of binding sites.

573

## 574 **Microscale thermophoresis/temperature-related intensity change measurements**

575 Microscale thermophoresis (MST) experiments were conducted measuring the temperature-  
576 related intensity change (TRIC) of the fluorescence signal<sup>68</sup>. A 12 bp fluorescently labelled  
577 dsDNA probe was generated by annealing a 5' FAM-labelled and an unlabelled strand  
578 (Microsynth; **Extended Data Table 4**) and used in all MST/TRIC experiments. Equilibrium  
579 binding assays were performed in 50 mM Tris-HCl pH 7.2, 50-150 mM NaCl, 0.05% (v/v)  
580 Tween-20. Increasing concentrations of purified wild-type or mutant FimT<sub>Lp</sub> samples were  
581 incubated with 100 nM of FAM-labelled 12 bp dsDNA probe at 25°C for 30 min prior to  
582 measurement. MST/TRIC measurements were performed at 20°C using a Monolith NT.115  
583 instrument (NanoTemper) at 25% LED power and 20% MST laser power. Curve fitting was



584 performed with data derived from the TRIC effect. For the experiment conducted with wild-  
585 type Fim<sub>T<sub>Lp</sub></sub> measured at 50 mM NaCl, the data appeared slightly biphasic in nature. This  
586 suggested the presence of two binding sites with similar, yet non-identical binding affinities.  
587 When these data were fitted with a binding model assuming two non-identical binding sites,  
588  $K_D(1)$  was indeed very similar to that obtained when fit according to two identical sites (~2.9  
589 vs 6.3  $\mu$ M). All other binding experiments using other methods (ITC and NMR), as well as  
590 MST/TRIC experiments conducted with Fim<sub>T<sub>Lp</sub></sub> mutants, did not reveal an obvious biphasic  
591 binding signature, which could be explained by insufficient resolution. Therefore, we chose  
592 to fit all data in the same manner, assuming two identical binding sites, to allow for their  
593 comparison. All MST/TRIC measurements were performed at least three times. In addition,  
594 all samples were measured twice, 30 min apart, resulting in very similar binding curves and  
595 derived dissociation constants, indicating that the binding equilibrium had been attained at  
596 the time of measurement.

597

### 598 **Transformation assay**

599 All transformation assays were performed with the *L. pneumophila* Lp02 strain in liquid  
600 medium at 30°C, similar to transformation assays performed by others<sup>10,69</sup>. Strains were  
601 streaked onto CYE solid medium from frozen stocks and incubated at 37°C for 3-4 days.  
602 From this plate, bacteria were resuspended in a liquid starter culture (5 mL of AYE medium)  
603 and incubated at 37°C overnight while shaking at 200 rpm. The starter culture was diluted  
604 into a fresh 10 mL AYE culture (starting OD<sub>600</sub> of 0.02) and cultured at 30°C while shaking.  
605 Once the culture reached an OD<sub>600</sub> of 0.3, 1 mL was transferred into a new tube and  
606 incubated with 1  $\mu$ g of transforming DNA at 30°C for a further 24 h. The transforming DNA  
607 consisted of a 4906 bp PCR product encompassing the *L. pneumophila* genomic region  
608 spanning *lpg2953-2958*, where the *hipB* gene (*lpg2955*) is interrupted by a kanamycin  
609 resistance cassette (based on<sup>70</sup>). This provides 2000 bp regions of homology up- and  
610 downstream of the resistance cassette. Tenfold serial dilutions of the culture were plated on  
611 selective (supplemented with 15  $\mu$ g/mL kanamycin) and non-selective CYE media. The  
612 plates were incubated at 37°C for 4-5 days and colony forming units (CFUs) were counted.  
613 The transformation efficiency corresponds to the ratio of the number of CFUs obtained on  
614 selective medium divided by the number of CFUs counted on non-selective medium. The  
615 minimum counting threshold was set at 10 colonies per plate. Transformation assays to test  
616 complementation of knockout strains with protein ectopically expressed from the pMMB207C  
617 plasmid were performed in the same manner, except for the addition of 0.5 mM IPTG during  
618 the incubation step of the bacteria with transforming DNA. Transformation assays requiring  
619 direct comparison between strains or complemented strains were performed in parallel.

620

## 621 **Western blot detection of pilin in sheared surface fractions**

622 Lp02 strains (parental,  $\Delta fimT$  and  $\Delta fimU$ ) harbouring pMMB207C-*pilA2-flag* were cultured at  
623 37°C for 24 h on CYE media, additionally supplemented with 0.5 mM IPTG. Cells were  
624 resuspended in AYE media containing a complete mini EDTA-free protease inhibitor cocktail  
625 tablet (Roche) and adjusted to an OD<sub>600</sub> of 20. To shear appendages from the cell surface,  
626 the resuspended cells were vortexed at maximal speed for 30 s. Subsequently, the  
627 depiliated cells were pelleted by two rounds of centrifugation at 20'000 g for 20 min at 4°C.  
628 The supernatants containing surface appendages, including T4P, were transferred to new  
629 tubes and the pellets were washed twice by resuspension in 1 mL AYE followed by  
630 centrifugation at 20'000 g for 20 min at 4°C. Both pellets and supernatants were separated  
631 by SDS-PAGE. Proteins were transferred to polyvinylidene fluoride (PVDF) membranes  
632 (Amersham) and PilA2-Flag was detected using a horse radish peroxidase (HRP)-coupled  
633 primary anti-Flag antibody at a 1:2000 dilution (Sigma, cat. no. SAB4200119). Enhanced  
634 chemiluminescence (ECL) (Cytiva) was used for the detection of the protein signal in a  
635 Amercham Imager 600. PVDF membranes were stained with Ponceau S to verify even  
636 loading across all lanes.

637

## 638 **Bioinformatic analyses**

### 639 *Collection of putative FimT and FimU sequences*

640 Three sets of FimT or FimU sequences were collected as follows: 1) a FimT set was  
641 retrieved by BlastP against FimT<sub>Lp</sub>, FimT<sub>Pa</sub>, FimT<sub>Ab</sub> and FimT<sub>Xc</sub> with a 95% query coverage  
642 cutoff, 2) a FimU set was retrieved by BlastP against FimU<sub>Lp</sub>, FimU<sub>Pa</sub>, FimU<sub>Ab</sub> and FimU<sub>Xc</sub>  
643 with a 95% (Pa, Ab, Xc) or 80% (Lp) query coverage cutoff, 3) a diverse FimT/U set was  
644 retrieved by a PSI-blast<sup>71</sup> search against FimT<sub>Lp</sub>, with >95% query coverage and e-value  
645 >0.005 cutoffs applied at each iteration, and the search continued for 8 iterations. To limit  
646 redundancy in the results all searches were conducted against the refseq\_select protein  
647 database which, for prokaryotes, contains only sequences from representative and reference  
648 genomes. The FimT and FimU sets were used for initial gene neighbourhood analyses  
649 beyond the four functionally characterised representatives (**Extended Data Fig. 6**), while the  
650 diverse set was used for phylogenetic analysis and to define conserved regions.

651

### 652 *Gene neighbourhood analysis*

653 The gene neighbourhood of each *fimT* and *fimU* was examined using custom Biopython<sup>72</sup>  
654 scripts and NCBI resources as follows 1) source genome(s) for each protein entry were  
655 identified from the Identical Protein Groups (IPG) resource (this was necessary because  
656 many of the blast results were non-redundant entries comprising multiple identical proteins),  
657 2) the genome region corresponding to the gene of interest and 5000 bp up- and

658 downstream was downloaded from the nucleotide database for one representative of each  
659 IPG (if <5000 bp flanking up- and downstream sequence was available the entry was  
660 excluded from further analysis), and 3) coding sequences in the neighbouring region were  
661 extracted as multifasta and searched against the Pfam<sup>73</sup> database of domain profiles using  
662 HMMER<sup>74</sup> (hmm scan function, e-value threshold 0.0001). *fimT* or *fimU* genes were  
663 classified as orphans or minor pilin locus components based on the presence of one or more  
664 of the Pfam domains PilC, PilX, PilX\_N and PilW in the flanking region. The presence of just  
665 one of these domains was defined as indicating a minor pilin locus, to account for the  
666 possibility that proteins only weakly matching the relevant Pfam domain would be missed, or  
667 that relevant proteins may be found >5000 bp away. NCBI scripts used in this study are  
668 available at [https://github.com/francesca-short/NCBI\\_scripts](https://github.com/francesca-short/NCBI_scripts).

669

#### 670 *Generation of high-confidence FimT set and phylogenetic analysis*

671 Because FimT is a GspH-domain protein and shares overall structural similarity with the type  
672 IV minor pilin FimU and the T2SS protein GspH, putative homologues from the diverse  
673 FimT/U set were filtered based on their gene neighbourhood to exclude likely *fimU* genes  
674 and generate a subset of high-confidence putative *fimT* genes for further analyses. As 100%  
675 of genes in the FimU set were located in minor pilin operons, orphan genes within the  
676 diverse FimT/U set were presumed to encode genuine FimT proteins, and these sequences  
677 were aligned along with FimT<sub>Lp</sub>, FimT<sub>Pa</sub>, FimT<sub>Ab</sub> and FimT<sub>Xc</sub> and used to generate a FimT  
678 HMM profile using HMMER<sup>74</sup> (hmmbuild function). A FimU HMM profile was generated from  
679 sequence set 2 (FimU homologues), following alignment with MUSCLE and removal of  
680 entries showing >80% amino acid identity to another entry. Each sequence from the diverse  
681 FimT/U set was scanned against both the FimU and FimT sequence HMMs and reported as  
682 a likely FimT if its match score to the FimT profile was >20 points greater than its match to  
683 the FimU profile. In this way, a set of 196 putative FimT protein sequences was obtained.  
684 FimT protein sequences were aligned using MUSCLE<sup>75</sup> with default (high-accuracy) settings,  
685 and the alignment was visualised and manually improved using JalView<sup>76</sup>. The FimT  
686 alignment was processed using TrimAL<sup>77</sup> to remove low-quality positions and uninformative  
687 sequences (parameters: -strictplus -resoverlap 0.8 -seqoverlap 75). A maximum-likelihood  
688 phylogenetic tree of the FimT homologues was constructed using IQtree<sup>78</sup> with the  
689 substitution model LG+F+R5<sup>79</sup> and ultrafast bootstrapping<sup>80</sup>. The phylogenetic tree and  
690 associated metadata was viewed using iTol<sup>81</sup>. The tree was midpoint-rooted and branches  
691 with less than 50% bootstrap support removed. Gene neighbourhood diagrams for selected  
692 FimT homologues were generated using Clinker<sup>82</sup>. The FimT motif diagram was generated  
693 using WebLogo<sup>83</sup>.

694

## 695 **Data availability**

696 The data that support the findings of this study are available from the corresponding author  
697 upon reasonable request. NMR spectra and corresponding model coordinates have been  
698 deposited in the **BioMag Resonance Data Bank (BMRB: XXX)** and Protein Data Bank (**PDB**  
699 **ID: XXXX**), respectively.

700

## 701 **References**

- 702 1. Johnsborg, O., Eldholm, V. & Håvarstein, L. S. Natural genetic transformation:  
703 prevalence, mechanisms and function. *Research in Microbiology* **158**, 767–778 (2007).
- 704 2. Johnston, C., Martin, B., Fichant, G., Polard, P. & Claverys, J.-P. Bacterial transformation:  
705 distribution, shared mechanisms and divergent control. *Nature reviews. Microbiology* **12**,  
706 181–196 (2014).
- 707 3. Stone, B. J. & Kwai, Y. A. Natural Competence for DNA Transformation by *Legionella*  
708 *pneumophila* and Its Association with Expression of Type IV Pili. *Journal of bacteriology*  
709 **181**, 1395–1402 (1999).
- 710 4. Gomez-Valero, L. *et al.* Extensive recombination events and horizontal gene transfer  
711 shaped the *Legionella pneumophila* genomes. *BMC Genomics* **12**, 536 (2011).
- 712 5. Sánchez-Busó, L., Comas, I., Jorques, G. & González-Candelas, F. Recombination drives  
713 genome evolution in outbreak-related *Legionella pneumophila* isolates. *Nat Genet* **46**, 1205–  
714 1211 (2014).
- 715 6. David, S. *et al.* Multiple major disease-associated clones of *Legionella pneumophila* have  
716 emerged recently and independently. *Genome Res* **26**, 1555–1564 (2016).
- 717 7. Newton, H. J., Ang, D. K. Y., Driel, I. R. van & Hartland, E. L. Molecular Pathogenesis of  
718 Infections Caused by *Legionella pneumophila*. *Clin Microbiol Rev* **23**, 274–298 (2010).
- 719 8. Cunha, P. B. A., Burillo, A. & Bouza, P. E. Legionnaires' disease. *The Lancet* **387**, 376–  
720 385 (2016).
- 721 9. Piepenbrink, K. H. DNA Uptake by Type IV Filaments. *Frontiers in Molecular*  
722 *Biosciences* **6**, 1441–13 (2019).
- 723 10. Hardy, L., Juan, P.-A., Coupat-Goutaland, B. & Charpentier, X. Transposon Insertion  
724 Sequencing in a Clinical Isolate of *Legionella pneumophila* Identifies Essential Genes and  
725 Determinants of Natural Transformation. *J Bacteriol* **203**, e00548-20 (2021).
- 726 11. Dubnau, D. & Blokesch, M. Mechanisms of DNA Uptake by Naturally Competent  
727 Bacteria. *Annual Review of Genetics* **53**, 217–237 (2019).
- 728 12. Jacobsen, T., Bardiaux, B., Francetic, O., Izadi-Pruneyre, N. & Nilges, M. Structure and  
729 function of minor pilins of type IV pili. *Medical Microbiology and Immunology* **209**, 301–  
730 308 (2020).

- 731 13. Berry, J.-L. & Pelicic, V. Exceptionally widespread nanomachines composed of type IV  
732 pilins: the prokaryotic Swiss Army knives. *FEMS Microbiology Reviews* **39**, 134–154 (2015).
- 733 14. Wolfgang, M. *et al.* PilT mutations lead to simultaneous defects in competence for natural  
734 transformation and twitching motility in piliated *Neisseria gonorrhoeae*. *Molecular*  
735 *Microbiology* **29**, 321–330 (1998).
- 736 15. Ellison, C. K. *et al.* Retraction of DNA-bound type IV competence pili initiates DNA  
737 uptake during natural transformation in *Vibrio cholerae*. *Nature Microbiology* **3**, 773–780  
738 (2018).
- 739 16. Seitz, P. & Blokesch, M. DNA-uptake machinery of naturally competent *Vibrio cholerae*.  
740 *Proceedings of the National Academy of Sciences* **110**, 17987–17992 (2013).
- 741 17. Weaver, S. J. *et al.* CryoEM structure of the type IVa pilus secretin required for natural  
742 competence in *Vibrio cholerae*. *Nat Commun* **11**, 5080 (2020).
- 743 18. Seitz, P. *et al.* ComEA Is Essential for the Transfer of External DNA into the Periplasm  
744 in Naturally Transformable *Vibrio cholerae* Cells. *PLoS Genet* **10**, e1004066-15 (2014).
- 745 19. Hepp, C. & Maier, B. Kinetics of DNA uptake during transformation provide evidence  
746 for a translocation ratchet mechanism. *Proceedings of the National Academy of Sciences* **113**,  
747 12467–12472 (2016).
- 748 20. Draskovic, I. & Dubnau, D. Biogenesis of a putative channel protein, ComEC, required  
749 for DNA uptake: membrane topology, oligomerization and formation of disulphide bonds.  
750 *Molecular microbiology* **55**, 881–896 (2004).
- 751 21. Attaiech, L. *et al.* Role of the Single-Stranded DNA–Binding Protein SsbB in  
752 Pneumococcal Transformation: Maintenance of a Reservoir for Genetic Plasticity. *Plos Genet*  
753 **7**, e1002156 (2011).
- 754 22. Bergé, M., Mortier-Barrière, I., Martin, B. & Claverys, J.-P. Transformation of  
755 *Streptococcus pneumoniae* relies on DprA- and RecA-dependent protection of incoming  
756 DNA single strands. *Molecular microbiology* **50**, 527–536 (2003).
- 757 23. Mortier-Barrière, I. *et al.* A Key Presynaptic Role in Transformation for a Widespread  
758 Bacterial Protein: DprA Conveys Incoming ssDNA to RecA. *Cell* **130**, 824–836 (2007).
- 759 24. Nero, T. M. *et al.* ComM is a hexameric helicase that promotes branch migration during  
760 natural transformation in diverse Gram-negative species. *Nucleic Acids Research* **46**, 6099–  
761 6111 (2018).
- 762 25. Schaik, E. J. van *et al.* DNA Binding: a Novel Function of *Pseudomonas aeruginosa*  
763 Type IV Pili. *Journal of bacteriology* **187**, 1455–1464 (2005).
- 764 26. Laurenceau, R. *et al.* A Type IV Pilus Mediates DNA Binding during Natural  
765 Transformation in *Streptococcus pneumoniae*. *PLoS pathogens* **9**, e1003473-12 (2013).

- 766 27. Cehovin, A. *et al.* Specific DNA recognition mediated by a type IV pilin. *Proceedings of*  
767 *the National Academy of Sciences* **110**, 3065–3070 (2013).
- 768 28. Berry, J.-L. *et al.* A Comparative Structure/Function Analysis of Two Type IV Pilin DNA  
769 Receptors Defines a Novel Mode of DNA Binding. *Structure* **24**, 926–934 (2016).
- 770 29. Salleh, M. Z. *et al.* Structure and Properties of a Natural Competence-Associated Pilin  
771 Suggest a Unique Pilus Tip-Associated DNA Receptor. *mBio* **10**, e00614-19 (2019).
- 772 30. Neuhaus, A. *et al.* Cryo-electron microscopy reveals two distinct type IV pili assembled  
773 by the same bacterium. *Nature Communications* 1–13 (2020) doi:10.1038/s41467-020-  
774 15650-w.
- 775 31. Goodman, S. D. & Scoocca, J. J. Identification and arrangement of the DNA sequence  
776 recognized in specific transformation of *Neisseria gonorrhoeae*. *Proc National Acad Sci* **85**,  
777 6982–6986 (1988).
- 778 32. Graves, J. F., Biswas, G. D. & Sparling, P. F. Sequence-specific DNA uptake in  
779 transformation of *Neisseria gonorrhoeae*. *J Bacteriol* **152**, 1071–1077 (1982).
- 780 33. Mell, J. C. & Redfield, R. J. Natural competence and the evolution of DNA uptake  
781 specificity. *Journal of bacteriology* **196**, 1471–1483 (2014).
- 782 34. Berry, J.-L., Cehovin, A., McDowell, M. A., Lea, S. M. & Pelicic, V. Functional Analysis  
783 of the Interdependence between DNA Uptake Sequence and Its Cognate ComP Receptor  
784 during Natural Transformation in *Neisseria* Species. *Plos Genet* **9**, e1004014 (2013).
- 785 35. Leong, C. G. *et al.* The role of core and accessory type IV pilus genes in natural  
786 transformation and twitching motility in the bacterium *Acinetobacter baylyi*. *PloS one* **12**,  
787 e0182139-25 (2017).
- 788 36. Giltner, C. L., Nguyen, Y. & Burrows, L. L. Type IV pilin proteins: versatile molecular  
789 modules. *Microbiology and molecular biology reviews : MMBR* **76**, 740–772 (2012).
- 790 37. Nguyen, Y. *et al.* *Pseudomonas aeruginosa* Minor Pilins Prime Type IVa Pilus Assembly  
791 and Promote Surface Display of the PilY1 Adhesin. *J Biol Chem* **290**, 601–611 (2015).
- 792 38. Craig, L., Pique, M. E. & Tainer, J. A. Type IV pilus structure and bacterial  
793 pathogenicity. *Nature reviews. Microbiology* **2**, 363–378 (2004).
- 794 39. Yanez, M. E., Korotkov, K. K., Abendroth, J. & Hol, W. G. J. Structure of the Minor  
795 Pseudopilin EpsH from the Type 2 Secretion System of *Vibrio cholerae*. *Journal of*  
796 *Molecular Biology* **377**, 91–103 (2008).
- 797 40. Raghunathan, K. *et al.* The 1.59 Å resolution structure of the minor pseudopilin EpsH of  
798 *Vibrio cholerae* reveals a long flexible loop. *Biochimica et Biophysica Acta (BBA) - Proteins*  
799 *and Proteomics* **1844**, 406–415 (2014).
- 800 41. Cierpicki, T. & Otlewski, J. Amide proton temperature coefficients as hydrogen bond  
801 indicators in proteins. *J Biomol Nmr* **21**, 249–261 (2001).

- 802 42. Corona, R. I. & Guo, J. Statistical analysis of structural determinants for protein-DNA-  
803 binding specificity. *Proteins* **84**, 1147–1161 (2016).
- 804 43. Douzi, B. *et al.* The XcpV/GspI Pseudopilin Has a Central Role in the Assembly of a  
805 Quaternary Complex within the T2SS Pseudopilus. *J Biol Chem* **284**, 34580–34589 (2009).
- 806 44. Korotkov, K. V. & Sandkvist, M. Protein Secretion in Bacteria. *Ecosal Plus* **8**, 227–244  
807 (2019).
- 808 45. Treuner-Lange, A. *et al.* PilY1 and minor pilins form a complex priming the type IVa  
809 pilus in *Myxococcus xanthus*. *Nat Commun* **11**, 5054 (2020).
- 810 46. Alm, R. A. & Mattick, J. S. Identification of two genes with prepilin-like leader  
811 sequences involved in type 4 fimbrial biogenesis in *Pseudomonas aeruginosa*. *J Bacteriol*  
812 **178**, 3809–3817 (1996).
- 813 47. Taguchi, F. & Ichinose, Y. Role of Type IV Pili in Virulence of *Pseudomonas syringae*  
814 pv. tabaci 6605: Correlation of Motility, Multidrug Resistance, and HR-Inducing Activity on  
815 a Nonhost Plant. *Mol Plant-microbe Interactions* **24**, 1001–1011 (2011).
- 816 48. Belete, B., Lu, H. & Wozniak, D. J. *Pseudomonas aeruginosa* AlgR Regulates Type IV  
817 Pilus Biosynthesis by Activating Transcription of the fimU-pilVWXY1Y2E Operon. *J*  
818 *Bacteriol* **190**, 2023–2030 (2008).
- 819 49. Douzi, B., Ball, G., Cambillau, C., Tegoni, M. & Voulhoux, R. Deciphering the Xcp  
820 *Pseudomonas aeruginosa* Type II Secretion Machinery through Multiple Interactions with  
821 Substrates. *J Biol Chem* **286**, 40792–40801 (2011).
- 822 50. Denise, R., Abby, S. S. & Rocha, E. P. C. The Evolution of Protein Secretion Systems by  
823 Co-option and Tinkering of Cellular Machineries. *Trends Microbiol* **28**, 372–386 (2020).
- 824 51. Korotkov, K. V. & Sandkvist, M. Architecture, Function, and Substrates of the Type II  
825 Secretion System. *Ecosal Plus* **8**, (2019).
- 826 52. DebRoy, S., Dao, J., Söderberg, M., Rossier, O. & Cianciotto, N. P. *Legionella*  
827 *pneumophila* type II secretome reveals unique exoproteins and a chitinase that promotes  
828 bacterial persistence in the lung. *Proc National Acad Sci* **103**, 19146–19151 (2006).
- 829 53. Lam, T. *et al.* Competence pili in *Streptococcus pneumoniae* are highly dynamic  
830 structures that retract to promote DNA uptake. *Mol Microbiol* 00: 1-16 (2021)  
831 doi:10.1111/mmi.14718.
- 832 54. Chung, Y. S. & Dubnau, D. All Seven comG Open Reading Frames Are Required for  
833 DNA Binding during Transformation of Competent *Bacillus subtilis*. *Journal of bacteriology*  
834 **180**, 41–45 (1998).
- 835 55. Laurenceau, R. *et al.* A Type IV Pilus Mediates DNA Binding during Natural  
836 Transformation in *Streptococcus pneumoniae*. *PLoS pathogens* **9**, e1003473-12 (2013).

- 837 56. Merriam, J. J., Mathur, R., Maxfield-Boumil, R. & Isberg, R. R. Analysis of the  
838 *Legionella pneumophila* flhI Gene: Intracellular Growth of a Defined Mutant Defective for  
839 Flagellum Biosynthesis. *Infection and immunity* **65**, 2497–2501 (1997).
- 840 57. Zuckman, D. M., Hung, J. B. & Roy, C. R. Pore-forming activity is not sufficient for  
841 *Legionella pneumophila* phagosome trafficking and intracellular growth. *Molecular*  
842 *microbiology* **32**, 990–1001 (1999).
- 843 58. Roy, C. R. & Isberg, R. R. Topology of *Legionella pneumophila* DotA: an Inner  
844 Membrane Protein Required for Replication in Macrophages. *Infection and immunity* **65**,  
845 571–578 (1997).
- 846 59. Berrow, N. S. *et al.* A versatile ligation-independent cloning method suitable for high-  
847 throughput expression screening applications. *Nucleic Acids Research* **35**, e45–e45 (2007).
- 848 60. Assenberg, R. *et al.* Expression, purification and crystallization of a lyssavirus matrix (M)  
849 protein. *Acta Crystallogr Sect F Struct Biology Cryst Commun* **64**, 258–262 (2008).
- 850 61. Chen, J. *et al.* *Legionella* Effectors That Promote Nonlytic Release from Protozoa.  
851 *Science* **303**, 1358–1361 (2004).
- 852 62. Muhandiram, D. R. & Kay, L. E. Gradient-Enhanced Triple-Resonance Three-  
853 Dimensional NMR Experiments with Improved Sensitivity. *J Magnetic Reson Ser B* **103**,  
854 203–216 (1994).
- 855 63. Kovacs, H. & Gossert, A. Improved NMR experiments with <sup>13</sup>C-isotropic mixing for  
856 assignment of aromatic and aliphatic side chains in labeled proteins. *J Biomol Nmr* **58**, 101–  
857 112 (2014).
- 858 64. Frueh, D. P. *et al.* Time-shared HSQC-NOESY for accurate distance constraints  
859 measured at high-field in <sup>15</sup>N-<sup>13</sup>C-ILV methyl labeled proteins. *J Biomol Nmr* **45**, 311  
860 (2009).
- 861 65. Vranken, W. F. *et al.* The CCPN data model for NMR spectroscopy: Development of a  
862 software pipeline. *Proteins Struct Funct Bioinform* **59**, 687–696 (2005).
- 863 66. Güntert, P. & Buchner, L. Combined automated NOE assignment and structure  
864 calculation with CYANA. *J Biomol Nmr* **62**, 453–471 (2015).
- 865 67. Case, D. A. *et al.* *Amber 2021*. (2021), Amber 2021, University of California, San  
866 Francisco.
- 867 68. López-Méndez, B. *et al.* Reproducibility and accuracy of microscale thermophoresis in  
868 the NanoTemper Monolith: a multi laboratory benchmark study. *Eur Biophys J* **50**, 411–427  
869 (2021).
- 870 69. Sexton, J. A. & Vogel, J. P. Regulation of hypercompetence in *Legionella pneumophila*.  
871 *Journal of bacteriology* **186**, 3814–3825 (2004).



- 872 70. Charpentier, X., Kay, E., Schneider, D. & Shuman, H. A. Antibiotics and UV radiation  
873 induce competence for natural transformation in *Legionella pneumophila*. *Journal of*  
874 *bacteriology* **193**, 1114–1121 (2011).
- 875 71. Schäffer, A. A. *et al.* Improving the accuracy of PSI-BLAST protein database searches  
876 with composition-based statistics and other refinements. *Nucleic Acids Res* **29**, 2994–3005  
877 (2001).
- 878 72. Cock, P. J. A. *et al.* Biopython: freely available Python tools for computational molecular  
879 biology and bioinformatics. *Bioinformatics* **25**, 1422–1423 (2009).
- 880 73. Mistry, J. *et al.* Pfam: The protein families database in 2021. *Nucleic Acids Res* **49**, D412-  
881 D419 (2020).
- 882 74. Eddy, S. R. Accelerated Profile HMM Searches. *Plos Comput Biol* **7**, e1002195 (2011).
- 883 75. Edgar, R. C. MUSCLE: a multiple sequence alignment method with reduced time and  
884 space complexity. *Bmc Bioinformatics* **5**, 113 (2004).
- 885 76. Waterhouse, A. M., Procter, J. B., Martin, D. M. A., Clamp, M. & Barton, G. J. Jalview  
886 Version 2—a multiple sequence alignment editor and analysis workbench. *Bioinformatics* **25**,  
887 1189–1191 (2009).
- 888 77. Capella-Gutiérrez, S., Silla-Martínez, J. M. & Gabaldón, T. trimAl: a tool for automated  
889 alignment trimming in large-scale phylogenetic analyses. *Bioinformatics* **25**, 1972–1973  
890 (2009).
- 891 78. Nguyen, L.-T., Schmidt, H. A., Haeseler, A. von & Minh, B. Q. IQ-TREE: A Fast and  
892 Effective Stochastic Algorithm for Estimating Maximum-Likelihood Phylogenies. *Mol Biol*  
893 *Evol* **32**, 268–274 (2015).
- 894 79. Kalyaanamoorthy, S., Minh, B. Q., Wong, T. K. F., Haeseler, A. von & Jermiin, L. S.  
895 ModelFinder: fast model selection for accurate phylogenetic estimates. *Nat Methods* **14**, 587–  
896 589 (2017).
- 897 80. Hoang, D. T., Chernomor, O., Haeseler, A. von, Minh, B. Q. & Vinh, L. S. UFBoot2:  
898 Improving the Ultrafast Bootstrap Approximation. *Mol Biol Evol* **35**, 518–522 (2017).
- 899 81. Letunic, I. & Bork, P. Interactive Tree Of Life (iTOL) v5: an online tool for phylogenetic  
900 tree display and annotation. *Nucleic Acids Res* **49**, W293-W296 (2021)  
901 doi:10.1093/nar/gkab301.
- 902 82. Gilchrist, C. L. M. & Chooi, Y.-H. clinker & clustermap.js: automatic generation of gene  
903 cluster comparison figures. *Bioinformatics* (2021) doi:10.1093/bioinformatics/btab007.
- 904 83. Crooks, G. E., Hon, G., Chandonia, J.-M. & Brenner, S. E. WebLogo: A Sequence Logo  
905 Generator. *Genome Res* **14**, 1188–1190 (2004).
- 906 84. Keene, O. N. The log transformation is special. *Stat Med* **14**, 811–819 (1995).

907 85. Landau, M. *et al.* ConSurf 2005: the projection of evolutionary conservation scores of  
908 residues on protein structures. *Nucleic Acids Res* **33**, W299–W302 (2005).

### 909 **Acknowledgements**

910 This work was funded by an SNSF PRIMA grant PR00P3\_179728 to MKH. FLS is supported  
911 by an Australian Research Council Discovery Early Career Research Award DE200101524.  
912 We would like to thank G. Waksman and A. Meir for the Lp02, CR019 and DH5 $\alpha$   $\lambda$ pir strains,  
913 and the pSR47S plasmid. We would also like to thank H. Hilbi for the pMMB207C plasmid.  
914 We are grateful to J. Scheuermann for the use of the VP-ITC instrument.

915

### 916 **Author Contributions**

917 SAGB cloned constructs, created *Legionella* strains, purified proteins, performed DNA  
918 binding studies, transformation assays, Western blots and analysed results. FLS designed  
919 and performed all bioinformatic analyses. SH constructed FimT chimera constructs and  
920 performed the corresponding transformation assays. MJMS purified proteins and performed  
921 ITC experiments. ADG performed and analysed all NMR-related experiments with help from  
922 SAGB. MKH designed and supervised the study, made figures and wrote the manuscript  
923 with help from all authors.

924

### 925 **Competing Interests Statement**

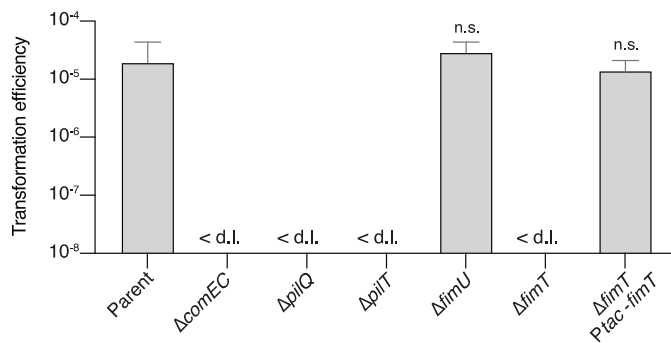
926 The authors declare no competing interests.

927

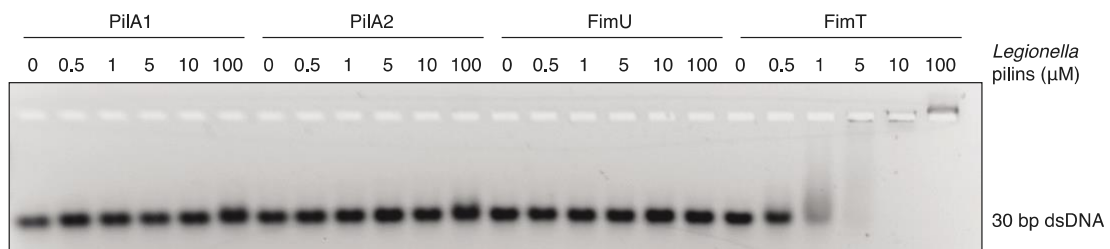
928 **Figures**

929

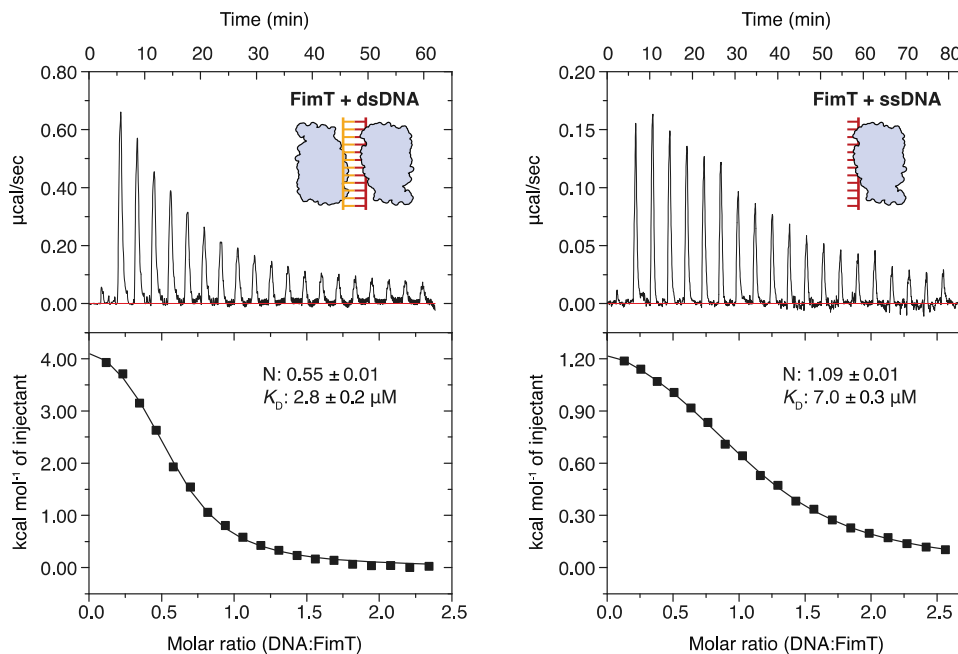
**a**



**b**



**c**



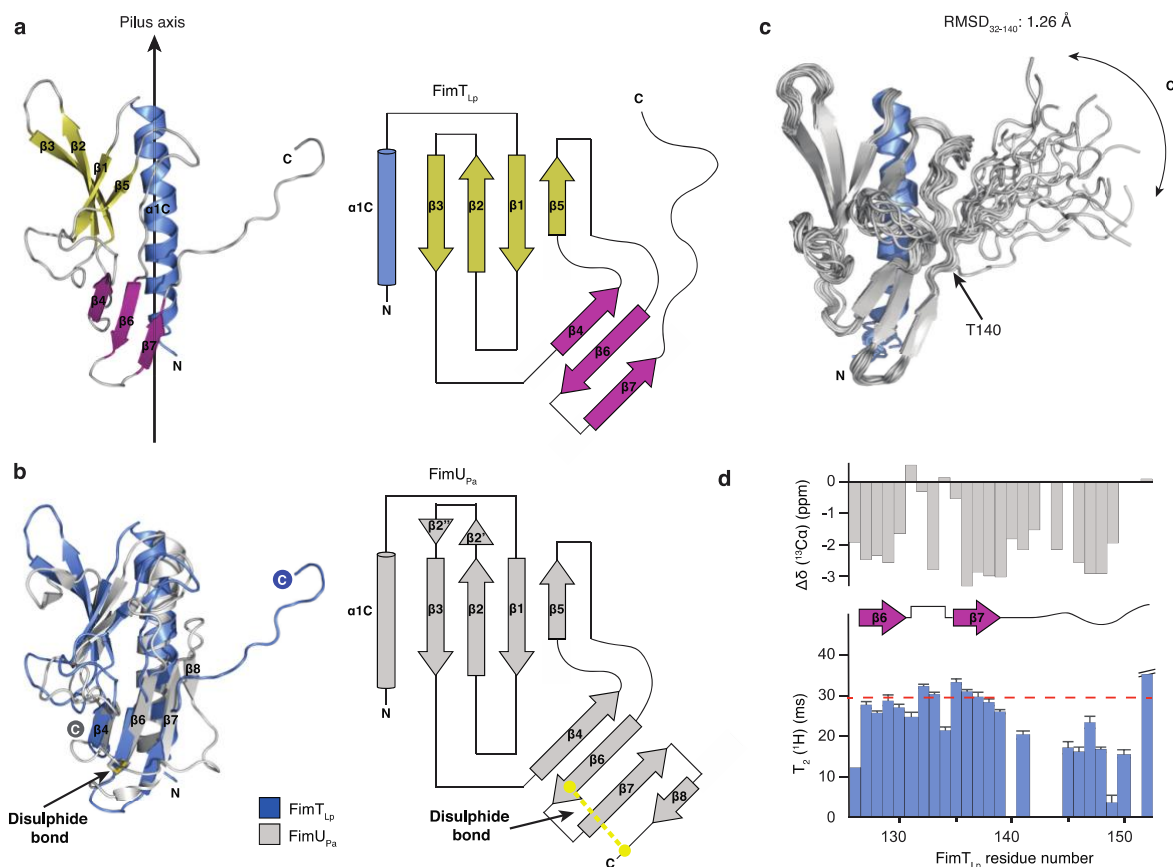
930

931

932 **Figure 1: FimT is critical for the transformation of *L. pneumophila* and binds to DNA**

933 **a**, Natural transformation efficiencies of the parental *L. pneumophila* Lp02 strain and Lp02  
 934 strains harbouring deletions of genes known to play a role in transformation compared to the  
 935 *fimU* and *fimT* deletion strains. The  $\Delta$ *fimT* strain was complemented by ectopic expression of  
 936 wild-type FimT, under the control of an IPTG-inducible promoter. The mean transformation  
 937 efficiencies of three independent biological replicates is shown (error bars represent

938 standard deviation [SD]). <d.l., below detection limit (d.l.) (average d.l. =  $2.0 \times 10^{-8} \pm 8.2$   
939  $\times 10^{-9}$ ). Statistical significances of transformation differences were determined on log-  
940 transformed<sup>84</sup> data using an unpaired t-test with Welch's correction. n.s., not statistically  
941 significant ( $p > 0.05$ ). **b**, *In vitro* DNA binding of purified *L. pneumophila* PilA1, PilA2, FimU  
942 and FimT assessed by an EMSA. A 30 bp dsDNA fragment (1  $\mu$ M) was incubated with  
943 increasing concentrations of purified pilins (0–100  $\mu$ M) and resolved by agarose gel  
944 electrophoresis. **c**, ITC binding studies of wild-type FimT binding to 12meric dsDNA (right)  
945 and ssDNA (left). In both cases, DNA (syringe) was injected into FimT (cell). Data were fitted  
946 using the “one set” of sites model, assuming that both binding sites on the dsDNA are of  
947 equal affinity.  
948



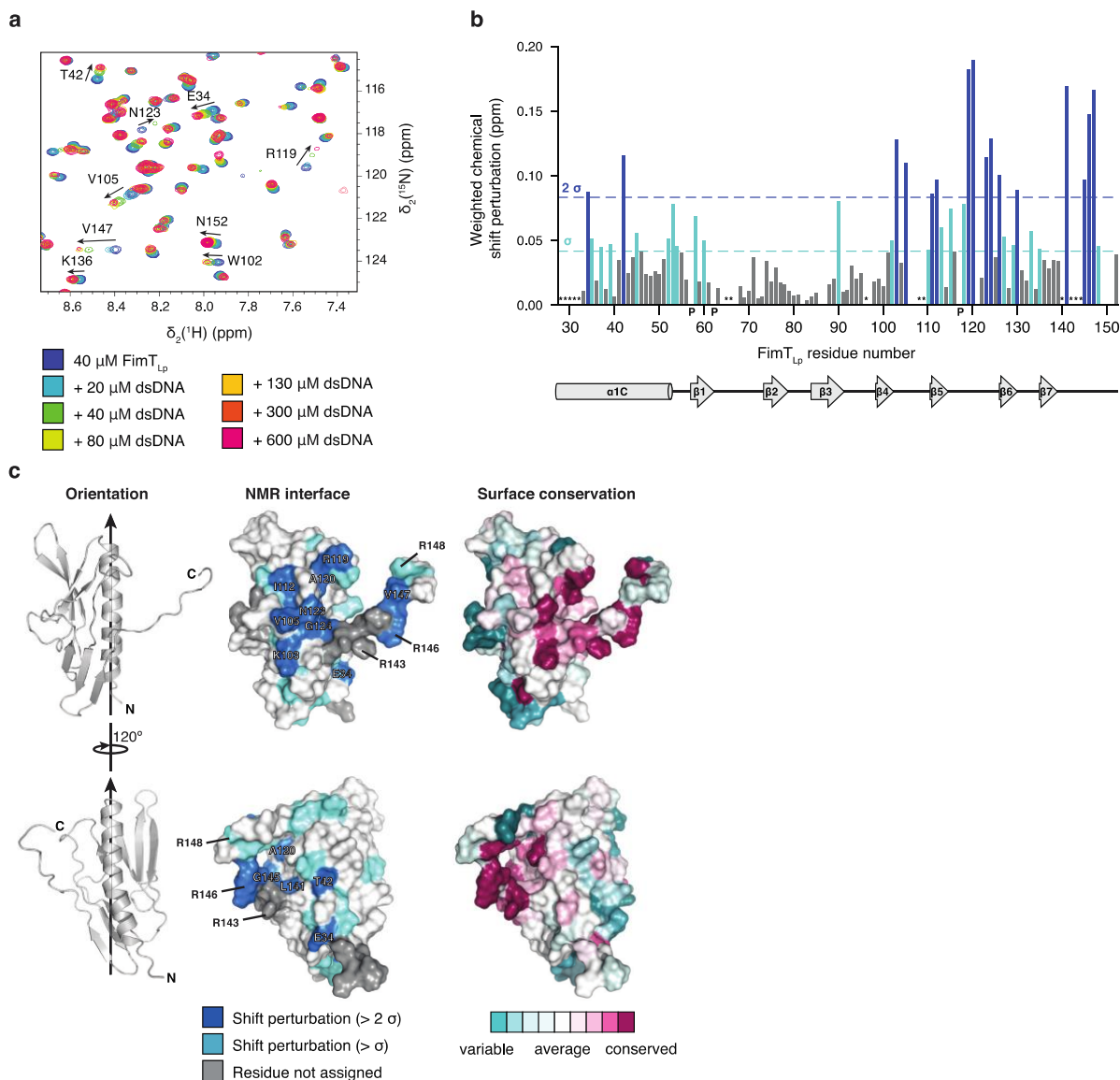
949

950

951 **Figure 2: The structure of FimT<sub>Lp</sub>**

952 **a**, The solution structure of FimT<sub>Lp</sub> 28-152 (state 18) in ribbon representation (left) and the  
 953 corresponding topology diagram (right). Secondary structure elements are indicated:  
 954 truncated N-terminal  $\alpha$ -helix ( $\alpha$ 1C) (blue),  $\beta$ -sheet I formed by  $\beta$ 1,  $\beta$ 2,  $\beta$ 3 and  $\beta$ 5 (yellow),  
 955 and  $\beta$ -sheet II formed by  $\beta$ 4,  $\beta$ 6 and  $\beta$ 7 (magenta). A vertical arrow indicates the pilus axis  
 956 from the cell surface towards the pilus tip. **b**, Structure alignment of FimT<sub>Lp</sub> (blue) and  
 957 FimU<sub>Pa</sub> (grey; PDB ID: 4IPV) (left) and the topology diagram of FimU<sub>Pa</sub> (right). The disulphide  
 958 bond of FimU<sub>Pa</sub> is indicated in stick representation with sulphur atoms in yellow. **c**,  
 959 Superimposed 20 lowest energy structures calculated by NMR spectroscopy. An arrow  
 960 indicates the conformational flexibility of the C-terminal tail (140-152). The pairwise  
 961 backbone root-mean-square deviation (RMSD) for the structured region (residues 32 to 140)  
 962 is 1.26 Å. N- and C-termini are indicated in each panel. **d**, C $\alpha$  chemical shift values (top) and  
 963 T<sub>2</sub>(<sup>1</sup>H) transverse relaxation data (bottom), encompassing the last 27 residues of FimT<sub>Lp</sub>.  
 964 Secondary structural elements are indicated and error bars represent the fitting errors of the  
 965 respective exponential decay curves.

966



967

968

969 **Figure 3: Identification of the DNA interaction surface of FimT<sub>Lp</sub>**

970 **a**, Selected region of <sup>1</sup>H, <sup>15</sup>N-HSQC spectra showing <sup>15</sup>N-labeled FimT<sub>Lp</sub> alone and  
 971 presence of increasing concentrations of 12 bp dsDNA. Full spectra are in **Source Data**. **b**,

972 Weighted CSP map generated from **a**. Residues experiencing CSPs ( $\Delta\text{ppm} > 1\sigma$ ), light  
 973 blue; residues experiencing CSPs ( $\Delta\text{ppm} > 2\sigma$ ), dark blue; P, prolines; \*, residues not

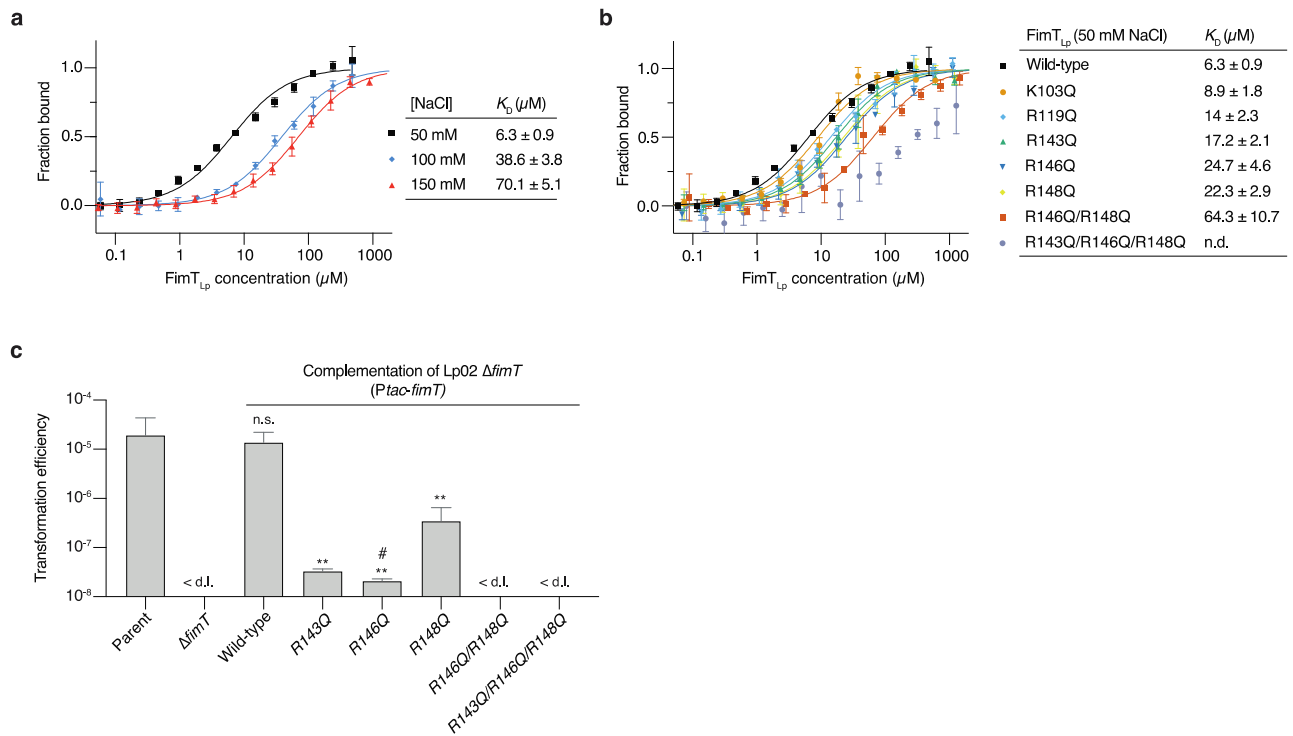
974 assigned. **c**, Left, FimT<sub>Lp</sub> is shown in two orientations rotated by 120° in ribbon

975 representation. Arrows indicate the pilus axis as in Fig. 2a. Middle, CSPs are mapped onto  
 976 the surface of FimT<sub>Lp</sub> and coloured as in **b**. Residues producing large shifts are labelled on

977 the molecular surface. Right, Surface residues of FimT<sub>Lp</sub> are coloured according to  
 978 conservation (full multisequence alignment in **Source Data**). This image was generated

979 using the ConSurf server<sup>85</sup>.

980



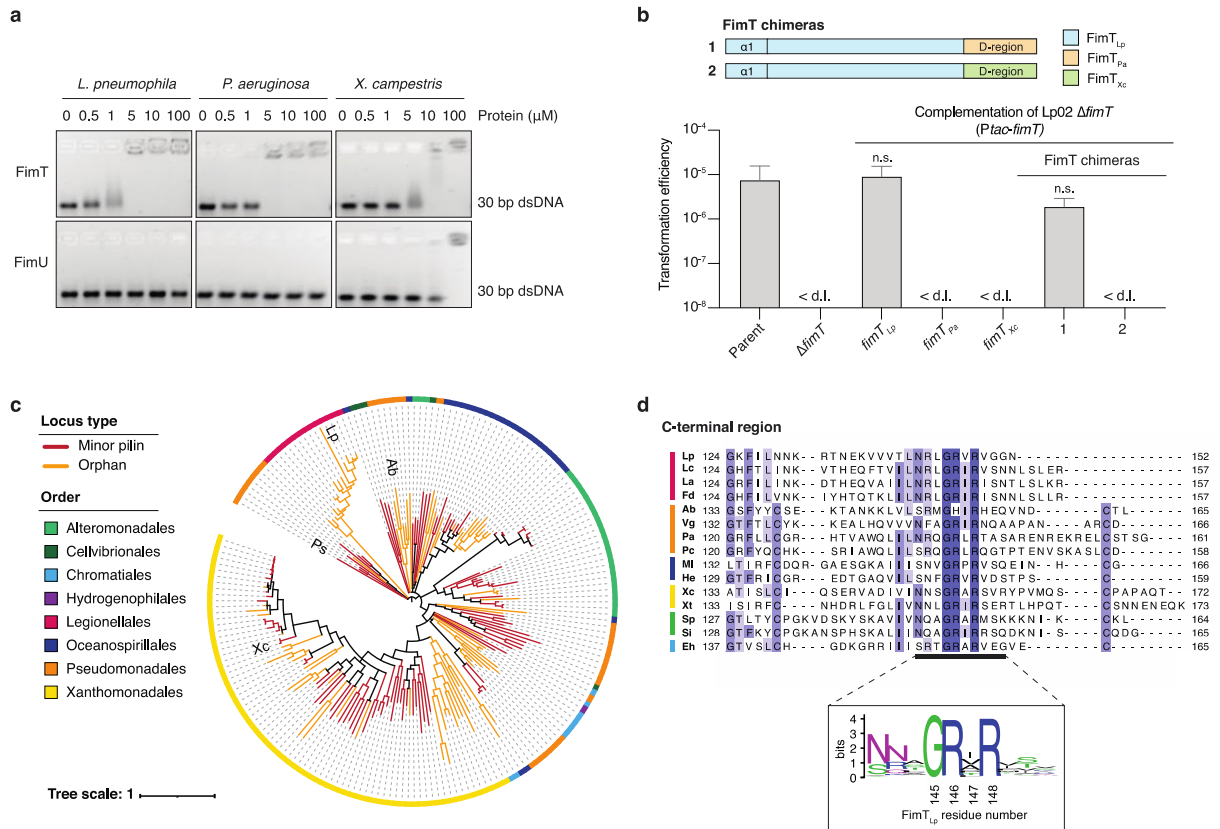
981

982

983 **Figure 4: Characterisation of FimT<sub>Lp</sub> binding to DNA *in vitro* and *in vivo***

984 MST/TRIC binding assay of 12 bp FAM-labelled dsDNA with **a**, wild-type FimT<sub>Lp</sub> performed  
 985 at increasing NaCl concentrations (ionic strength) and **b**, wild-type FimT<sub>Lp</sub> compared to FimT  
 986 mutants. n.d., not determined. The MST/TRIC data were fitted according to two binding sites  
 987 with equal affinity. Error bars represent the mean  $\pm$  SD. **c**, Natural transformation efficiencies  
 988 of parental Lp02, Lp02  $\Delta fimT$ , and the Lp02  $\Delta fimT$  strain complemented by ectopic  
 989 expression of wild-type and FimT<sub>Lp</sub> mutants. The mean transformation efficiencies of three  
 990 independent biological replicates are plotted with error bars representing the SD. <d.l., below  
 991 d.l. (average d.l. =  $2.0 \times 10^{-8} \pm 8.2 \times 10^{-9}$ ); #, below d.l. in at least one replicate (average d.l.  
 992 used to calculate the mean transformation efficiency). These assays were performed in  
 993 parallel to those displayed in Fig. 1a, and statistical differences were determined on log-  
 994 transformed data using an unpaired t-test with Welch's correction. \*\*,  $p < 0.01$ ; n.s., not  
 995 statistically significant ( $p > 0.05$ ).

996



997

998

999

## Figure 5: Bioinformatic and functional analysis of FimT orthologues

1000 **a**, EMSA showing *in vitro* DNA binding of purified FimT and FimU orthologues from

1001 *L. pneumophila*, *P. aeruginosa* and *X. campestris*. A 30 bp dsDNA fragment (1 μM) was

1002 incubated with increasing concentrations of purified pilins (0-100 μM) and resolved by

1003 agarose gel electrophoresis. **b**, A comparison of natural transformation efficiencies of the

1004 Lp02 ΔfimT strain complemented by ectopic expression of FimT<sub>Lp</sub>, FimT orthologues from

1005 *P. aeruginosa* (FimT<sub>Pa</sub>) and *X. campestris* (FimT<sub>Xc</sub>), or chimeric FimT mutants (1-2). The

1006 corresponding composition of these FimT chimeras (1-2) is explained by a schematic

1007 drawing (top). The mean transformation frequencies of three independent biological

1008 replicates are shown with error bars representing the SD. <d.l., below d.l. (average d.l. = 4.8

1009 x 10<sup>-8</sup> ± 2.1 x 10<sup>-8</sup>). An unpaired t-test with Welch's correction, using log-transformed data,

1010 was used to analyse statistical significance. n.s., not statistically significant (p>0.05). **c**,

1011 Phylogenetic tree of FimT homologues, comprising eight orders of γ-proteobacteria

1012 illustrated by the coloured circumferential ring. Branches coloured in orange represent FimTs

1013 encoded as orphan genes, whereas those coloured red represent FimTs encoded within

1014 minor pilin operons. The positions of the four functionally characterised FimT orthologues in

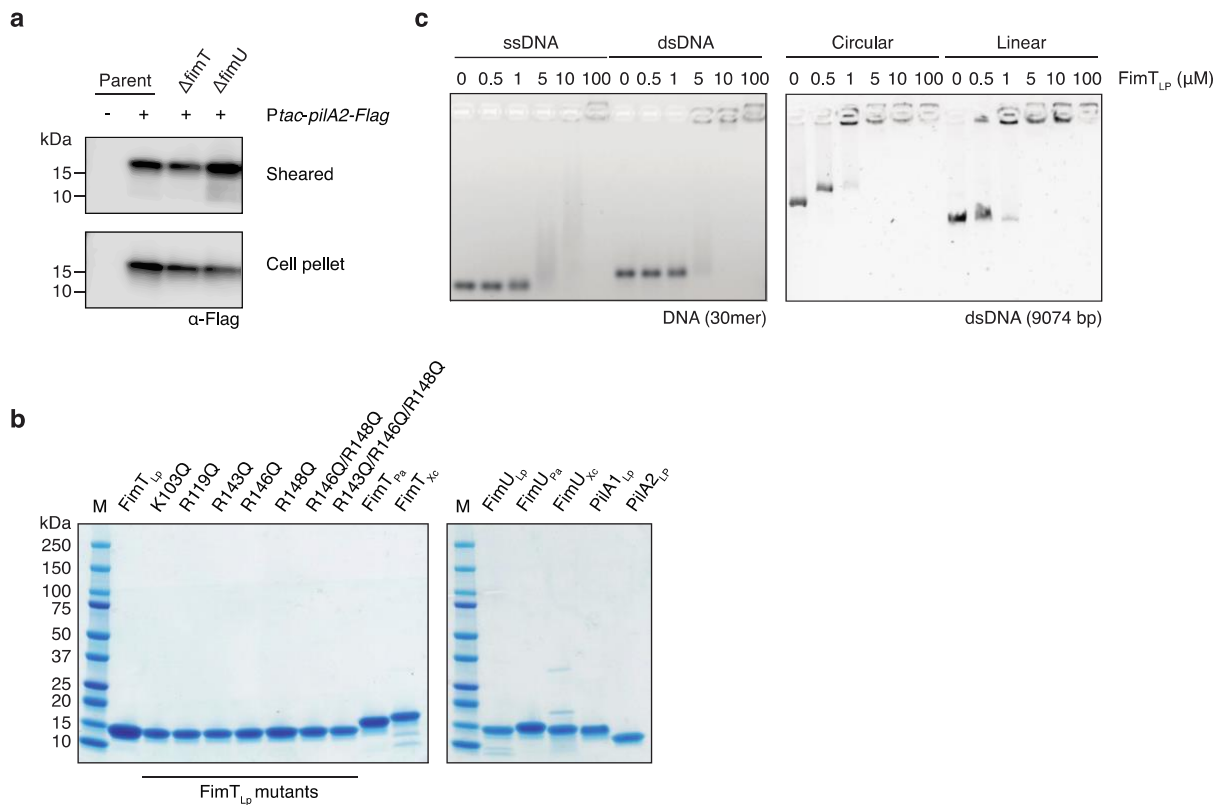
1015 the tree are indicated (Lp, *L. pneumophila*; Ab, *A. baylyi*; Pa, *P. aeruginosa*; and Xc,



1016 *X. campestris*). The scale bar indicates the average number of substitutions per site. **d**, Top,  
1017 multisequence alignment of representative FimT orthologues across six orders (indicated by  
1018 a coloured line as in c) focusing on their C-terminal region (Lc, *Legionella cherrii*; La,  
1019 *Legionella anisa*; Fd, *Fluoribacter dumoffii*; Vg, *Ventrosimonas gracilis*; Pc, *Pseudomonas*  
1020 *chloritidismutans*; Ml, *Marinicella litoralis*; He, *Halomonas endophytica*; Xt, *Xylella*  
1021 *taiwanensis*; Sp, *Shewanella polaris*; Si, *Shewanella indica*; Eh, *Ectothiorhodospira*  
1022 *haloalkaliphile*). Residues are coloured according to sequence identity. Bottom, sequence  
1023 logo generated from the full multisequence alignment of 196 high-confidence FimTs (**Source**  
1024 **Data**).  
1025

1026 **Extended Data**

1027



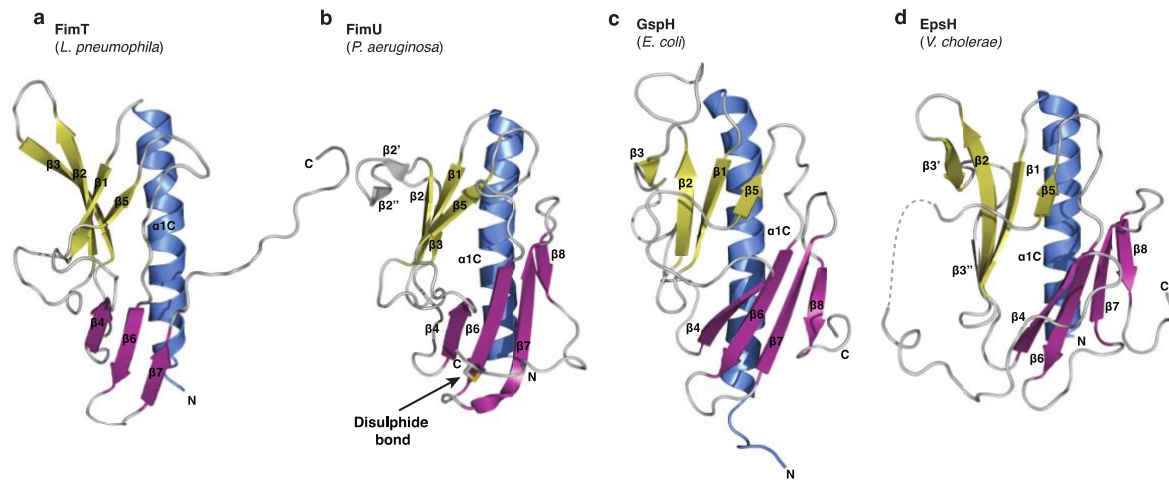
1028

1029

1030 **Extended Data Figure 1: Cell surface expression of PiiA2-Flag, *in vitro* DNA binding of**  
 1031 **FimT<sub>Lp</sub> and purified proteins utilised in this study**

1032 **a**, Immunodetection of ectopically expressed PiiA2-Flag in various Lp02 strains using anti-  
 1033 Flag antibodies (**Source Data**). Sheared pili were detected in supernatants (sheared) and  
 1034 the whole cell lysates of depiliated cells (cell pellet). **b**, All purified N-terminally truncated  
 1035 pilins (construct boundaries can be found in **Extended Data Table 3**), utilised in this study,  
 1036 resolved by SDS-PAGE. M, marker; Lp, *L. pneumophila*; Pa, *P. aeruginosa*; Xc,  
 1037 *X. campestris*. **c**, EMSAs showing *in vitro* DNA binding of FimT<sub>Lp</sub> to ssDNA vs dsDNA (left)  
 1038 and linear vs circular DNA (right). DNA probes were incubated with increasing  
 1039 concentrations of FimT<sub>Lp</sub> and resolved by agarose gel electrophoresis.

1040



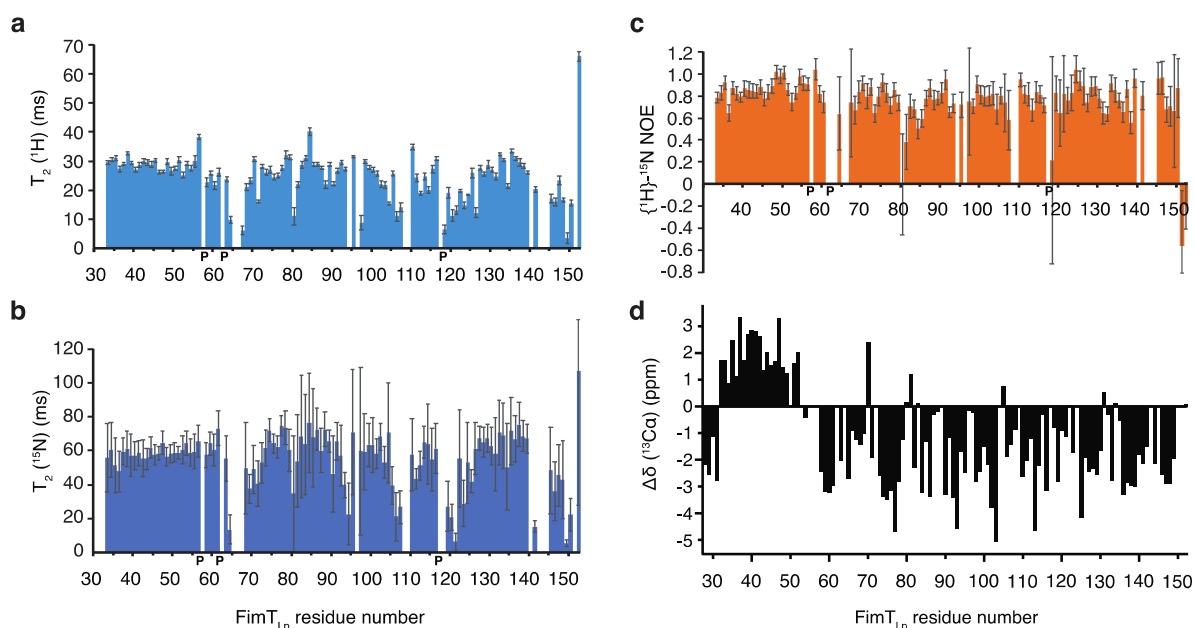
1041

1042

1043 **Extended Data Figure 2: Structures of GspH/FimT family members**

1044 **a**, The structure of FimT from *L. pneumophila* (state 18, this study); **b**, FimU from  
1045 *P. aeruginosa* (PDB ID: 4IPV); **c**, GspH from *E. coli* (state 1, PDB ID: 2KNQ); and **d**, EpsH  
1046 from *V. cholerae* (PDB ID: 2QV8). The FimT<sub>Lp</sub> and GspH<sub>Ec</sub> structures were determined using  
1047 NMR spectroscopy, while those of FimU<sub>Pa</sub> and EpsH<sub>Vc</sub> are crystal structures. The disulphide  
1048 bond of FimU is shown in stick representation (sulphur atoms in yellow), indicated by an  
1049 arrow. The previously named  $\beta 3$  and  $\beta 4$ -strands of the EpsH structure<sup>1</sup> have been labelled  
1050 as  $\beta 3'$  and  $\beta 3''$  for consistency of strand nomenclature across all depicted structures. All  
1051 structures are shown in ribbon representation with their N-and C-termini indicated and  
1052 secondary structural elements are coloured and labelled as in Fig. 2a.

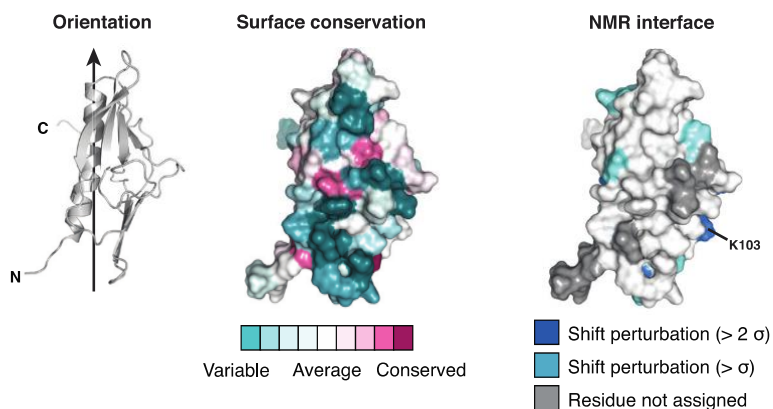
1053



1054  
1055

1056 **Extended Data Figure 3: Relaxation data for FimT<sub>Lp</sub> indicate dynamics of the**  
1057 **C-terminal residues 140–150 on the millisecond timescale**

1058 **a, b**, Backbone amide T<sub>2</sub> transverse relaxation data of FimT<sub>Lp</sub> for <sup>1</sup>H (**a**) and <sup>15</sup>N (**b**) nuclei,  
1059 where amide groups of the loops and the C-terminus show significantly decreased T<sub>2</sub> values  
1060 compared to the folded part of the domain. The low T<sub>2</sub> values for the C-terminal tail (signals  
1061 of amides of residues 140 and 142–144 were too weak to be analysed), indicate dynamics of  
1062 the C-terminal residues (140–150) on the microsecond to millisecond timescale. Proline  
1063 residues are indicated with a bold letter P. Error bars represent the fitting errors of the  
1064 respective exponential decay curves. **c**, Heteronuclear {<sup>1</sup>H}-<sup>15</sup>N NOE data show that only the  
1065 last two residues (151 and 152) exhibit fast dynamics on the nanosecond timescale, typical  
1066 for flexibly disordered termini. Error bars reflect the error from the signal-to-noise ratio of the  
1067 individual signals used for the analysis. **d**, C<sub>α</sub> chemical shift deviation from random coil  
1068 values (Δδ(<sup>13</sup>Ca)) indicate predominantly β-strand secondary structure for the C-terminal  
1069 residues. Significant (>0.5 ppm) positive and negative deviations of <sup>13</sup>C<sub>α</sub> chemical shifts  
1070 from random coil values indicate α-helical and β-strand conformations of the backbone,  
1071 respectively. <sup>13</sup>C<sub>α</sub> chemical shifts are shown without smoothing, representing the raw data  
1072 after calibration of the <sup>13</sup>C chemical shift to 2,2-dimethyl-2-silapentane-5-sulfonate (DSS).  
1073



1074

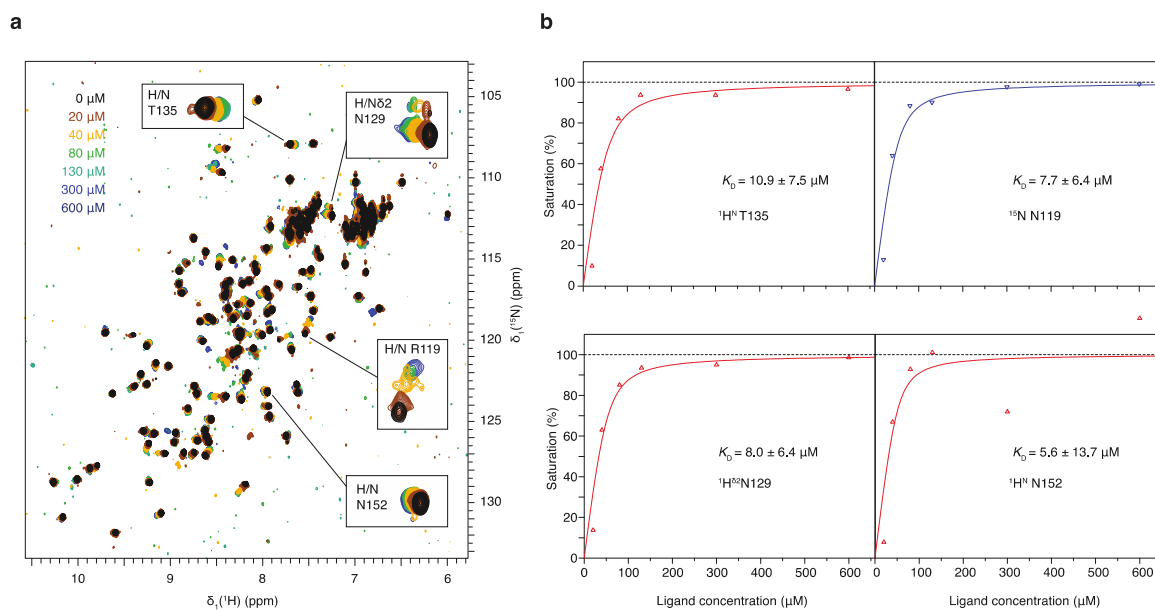
1075

1076 **Extended Data Figure 4: NMR binding studies of FimT<sub>Lp</sub> to DNA**

1077 Left, FimT<sub>Lp</sub> is shown in ribbon representation rotated a further 120° with respect to the  
1078 orientations displayed in Fig. 3c. Middle, residues experiencing chemical shift perturbations  
1079 due to DNA binding are mapped onto the surface of FimT<sub>Lp</sub>. Right, surface residues of  
1080 FimT<sub>Lp</sub> are coloured according to conservation.

1081

1082



1083

1084

1085 **Extended Data Figure 5: Affinity determination of FimT to 12 bp dsDNA by NMR**

1086 **a**, DNA binding studies of FimT<sub>LP</sub> performed by NMR spectroscopy. Increasing

1087 concentrations of 12 bp dsDNA (see colour code on top left in spectra overlay) were added

1088 to 40  $\mu\text{M}$  of  $^{15}\text{N}$ -labelled FimT<sub>LP</sub> and the CSPs of four peaks were plotted against the ligand

1089 (12 bp DNA) concentration. **b**, For the four signals indicated in the spectra overlay, the

1090 binding curves are shown on the right-hand side, for  $^1\text{H}$  and  $^{15}\text{N}$  nuclei in red and blue

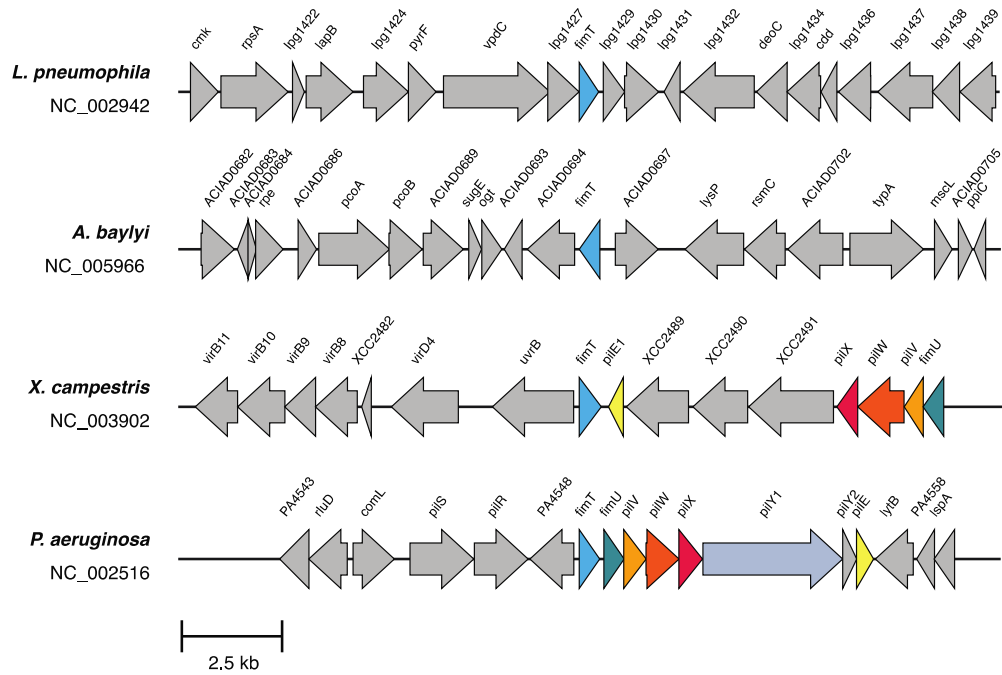
1091 triangles, respectively. The data were fitted assuming two identical binding sites (solid lines)

1092 and averaged to estimate a  $K_D$  of  $\sim 8 \mu\text{M}$  of the interaction.

1093

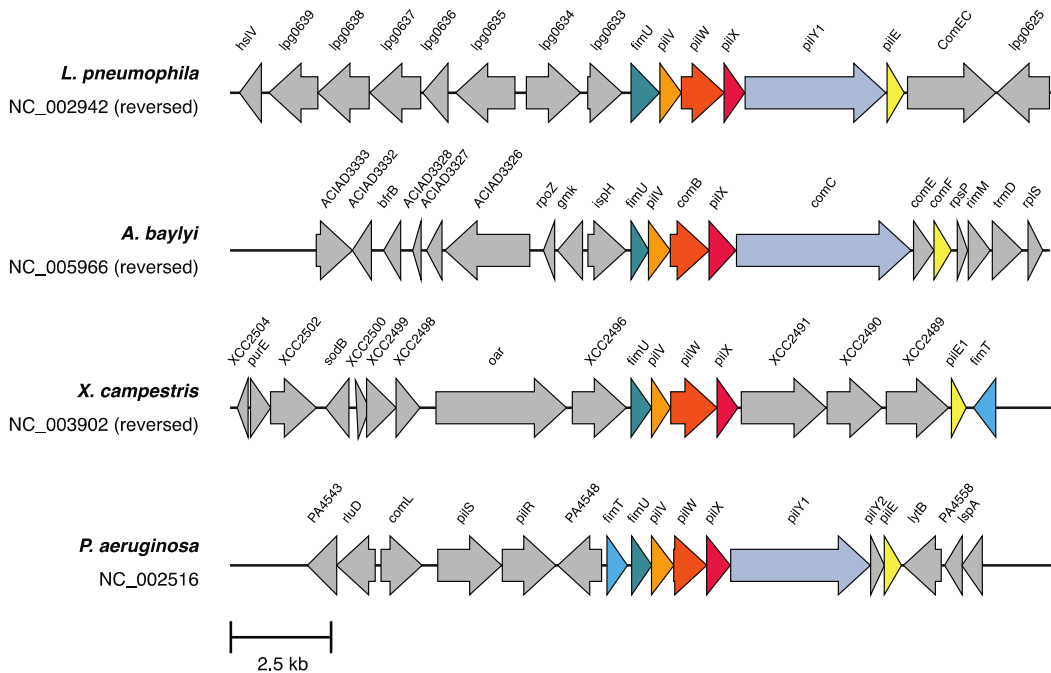
**a**

**Gene neighbourhood: FimT**



**b**

**Gene neighbourhood: FimU**



1094

1095

1096 **Extended Data Figure 6: Gene neighbourhoods of FimT and FimU**

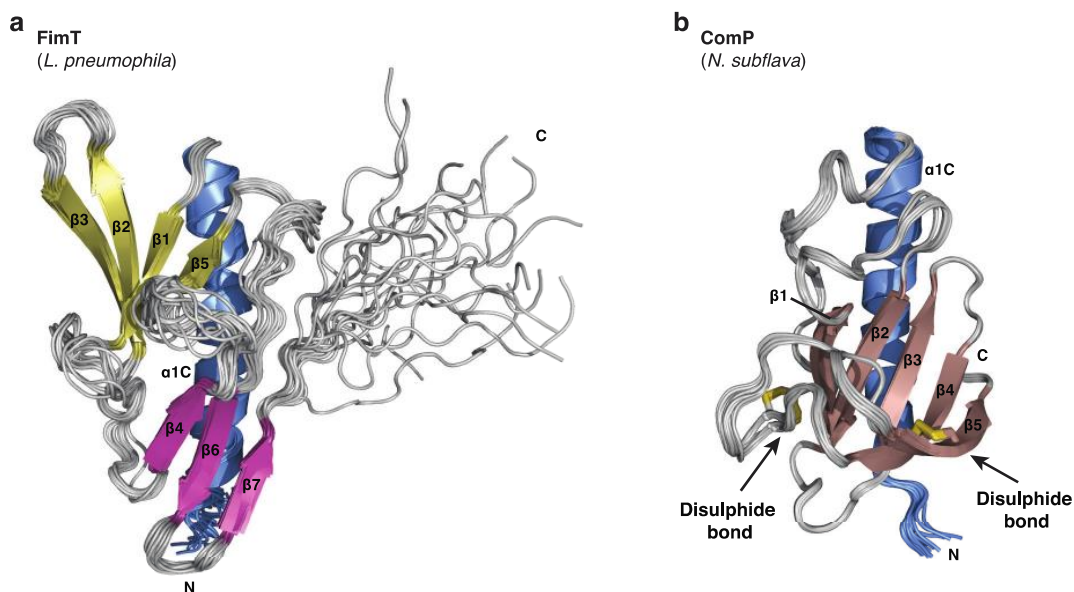
1097 Genomic regions around FimT (a) and FimU (b) in *L. pneumophila*, *A. baylyi*, *X. campestris*

1098 and *P. aeruginosa*. Each gene is labelled with its name or locus tag (if unannotated). Genes

1099 coding for T4P homologues are colour-coded identically across the different bacterial

1100 species. Among FimT and FimU homologues collected by BlastP using the four  
1101 representative sequences, 25% of FimT sequences were located close to other minor pilin  
1102 operon components, while 100% of FimU sequences were located in minor pilin operons  
1103 (see **Source Data**).  
1104





1105

1106

1107 **Extended Data Figure 7: Comparison of the NMR structures of FimT and ComP**

1108 **a, b**, Superimposed 20 lowest energy structures calculated by NMR spectroscopy of FimT  
1109 from *L. pneumophila* (**a**) and ComP from *Neisseria subflava* (PDB ID: 2NBA<sup>3</sup>) (**b**). The DD-  
1110 region defining disulphide bonds of ComP are shown in stick representation (sulphur atoms  
1111 in yellow) and are indicated by arrows. Both structures are shown in ribbon representation  
1112 with their N-and C-termini indicated.

1113

1114 **Extended Data Table 1 NMR and refinement statistics for FimT<sub>Lp</sub>**

	<b>FimT<sub>Lp</sub></b>
<b>NMR distance and dihedral constraints</b>	
Distance constraints	
Total NOE	2311
Intra-residue	635
Inter-residue	1676
Sequential ( $ i - j  = 1$ )	522
Medium-range ( $ i - j  < 4$ )	344
Long-range ( $ i - j  > 5$ )	810
Hydrogen bonds	-
Total dihedral angle restraints*	
Backbone	666
Other	558
<b>Structure statistics</b>	
Average Cyana target function	0.21 ± 0.02
Violations (mean and s.d.)**	
Distance constraints (Å)	0
Max. dihedral angle violation (°)	123.98 ± 28.54
Max. distance constraint violation (Å)	0.57 ± 0.19
Deviations from idealized geometry	
Bond lengths (Å)	0.0035 ± 0.0012
Bond angles (°)	1.377 ± 0.459
Average pairwise r.m.s. deviation*** (Å)	
Heavy	1.13 ± 0.13
Backbone	0.56 ± 0.16

1115

1116 \* Dihedral angle restraints were derived from C $\alpha$  chemical shifts using TALOS+ as  
1117 implemented in cyana 3.98

1118 \*\* Restraints violated in 6 or more structures

1119 \*\*\* Pairwise r.m.s. deviation for structured regions (res. 32–62, 70–139) was calculated  
1120 among 20 refined structures.

1121

1122 **Extended Data Table 2: Strains used in this study**

Name	Relevant genotype/description	Source/Reference
<i>Escherichia coli</i>		
BL21 (DE3)	<i>E. coli</i> expression strain	NEB (cat. no. C2527H/I)
Shuffle T7	<i>E. coli</i> expression strain	NEB (cat. no. C3026J)
Stellar (HST08 strain)	<i>E. coli</i> cloning strain	Takara (cat. no. 636763/636766)
DH5 $\alpha$ $\lambda$ pir	<i>E. coli</i> cloning strain: Encodes $\pi$ protein for the replication of the <i>pir</i> - dependent origin of replication - <i>oriR(R6K)</i>	4,5
CR019	<i>E. coli</i> mobilizing strain: MT607 <i>E. coli</i> containing pRK600 plasmid [ <i>oriR</i> (ColE1) <i>oriT</i> (RK2); CmR]	6
<i>Legionella pneumophila</i>		
Lp02 WT	Philadelphia-1 <i>rpsL hsdR thyA</i> ; SmR	7
Lp02 $\Delta$ <i>fimT</i>	Lp02 $\Delta$ <i>fimT</i> ( <i>lpg1428</i> )	This study
Lp02 $\Delta$ <i>fimU</i>	Lp02 $\Delta$ <i>fimU</i> ( <i>lpg0632</i> )	This study
Lp02 $\Delta$ <i>pilQ</i>	Lp02 $\Delta$ <i>pilQ</i> ( <i>lpg0931</i> )	This study
Lp02 $\Delta$ <i>pilT</i>	Lp02 $\Delta$ <i>pilT</i> ( <i>lpg2013</i> )	This study
Lp02 $\Delta$ <i>comEC</i>	Lp02 $\Delta$ <i>comEC</i> ( <i>lpg0626</i> )	This study

1123

1124

1125 **Extended Data Table 3: Plasmids used in this study**

Name	Relevant genotype/description	Source/Reference
pMMB207C	<i>Legionella</i> expression vector derived from RSF1010: IncQ lacI <sup>q</sup> P <sub>tac</sub> oriT Δ <i>mobA</i> ; CmR	8
pMMB207C- <i>fimT</i> <sub>Lp</sub>	<i>L. pneumophila</i> wild-type <i>fimT</i>	This study
pMMB207C- <i>fimT</i> <sub>Lp</sub> R143Q	pMMB207C- <i>fimT</i> <sub>Lp</sub> , with <i>fimT</i> R143Q mutation	This study
pMMB207C- <i>fimT</i> <sub>Lp</sub> R146Q	pMMB207C- <i>fimT</i> <sub>Lp</sub> , with <i>fimT</i> R146Q mutation	This study
pMMB207C- <i>fimT</i> <sub>Lp</sub> R148Q	pMMB207C- <i>fimT</i> <sub>Lp</sub> , with <i>fimT</i> R148Q mutation	This study
pMMB207C- <i>fimT</i> <sub>Lp</sub> R146Q, R148Q	pMMB207C- <i>fimT</i> <sub>Lp</sub> , with <i>fimT</i> R146Q, R148Q mutations	This study
pMMB207C- <i>fimT</i> <sub>Lp</sub> R143Q, R146Q, R148Q	pMMB207C- <i>fimT</i> <sub>Lp</sub> , with <i>fimT</i> R143Q, R146Q, R148Q mutations	This study
pMMB207C- <i>pilA2</i> -flag	<i>L. pneumophila pilA2</i> ( <i>lpg1915</i> )-flag	This study
pMMB207C- <i>fimT</i> <sub>Pa</sub>	<i>Pseudomonas aeruginosa</i> PAO1 <i>fimT</i> (PA4549)	This study
pMMB207C- <i>fimT</i> <sub>chimera 1</sub>	pMMB207C- <i>fimT</i> <sub>Lp</sub> residues 1-128, fused to <i>fimT</i> <sub>Pa</sub> residues 125-161	This study
pMMB207C- <i>fimT</i> <sub>Xc</sub>	<i>Xanthomonas campestris</i> ATCC 33913 <i>fimT</i> (XCC2486)	This study
pMMB207C- <i>fimT</i> <sub>chimera 2</sub>	pMMB207C- <i>fimT</i> <sub>Lp</sub> residues 1-128, fused to <i>fimT</i> <sub>Xc</sub> residues 138-172	This study
pSR47S	Suicide plasmid: <i>oriR</i> (R6K) <i>oriT</i> (RP4) <i>sacB</i> ; KanR	Vogel, J. P., et al. (unpublished data) 9
pSR47S- <i>fimT</i>	<i>L. pneumophila fimT</i> gene with 1000 bp up- and downstream sequence (homology regions)	This study
pSR47S- <i>fimU</i>	<i>L. pneumophila fimU</i> gene with 1000 bp up- and downstream sequence (homology regions)	This study
pSR47S- <i>pilQ</i>	<i>L. pneumophila pilQ</i> gene with 1000 bp up- and downstream sequence (homology regions)	This study
pSR47S- <i>pilT</i>	<i>L. pneumophila pilT</i> gene with 1000 bp up- and downstream sequence (homology regions)	This study
pSR47S- <i>comEC</i>	<i>L. pneumophila comEC</i> gene with 1000 bp up- and downstream sequence (homology regions)	This study
pSR47S-Δ <i>fimT</i>	pSR47S- <i>fimT</i> , with <i>fimT</i> deletion	This study
pSR47S-Δ <i>fimU</i>	pSR47S- <i>fimU</i> , with <i>fimU</i> deletion (52 nt left intact at 5' end of gene)	This study
pSR47S-Δ <i>pilQ</i>	pSR47S- <i>pilQ</i> , with <i>pilQ</i> deletion	This study
pSR47S-Δ <i>pilT</i>	pSR47S- <i>pilT</i> , with <i>pilT</i> deletion	This study
pSR47S-Δ <i>comEC</i>	pSR47S- <i>comEC</i> , with <i>comEC</i> deletion	This study
pOPINS	<i>E. coli</i> expression vector: N-terminal His <sub>6</sub> -SUMO tag, T7 promoter; KanR	10
pOPINS- <i>fimT</i> <sub>Lp</sub>	<i>L. pneumophila</i> wild-type <i>fimT</i> , residues 28-152	This study
pOPINS- <i>fimT</i> <sub>Lp</sub> K103Q	pOPINS- <i>fimT</i> <sub>Lp</sub> , with <i>fimT</i> K103Q mutation	This study
pOPINS- <i>fimT</i> <sub>Lp</sub> R119Q	pOPINS- <i>fimT</i> <sub>Lp</sub> , with <i>fimT</i> R119Q mutation	This study
pOPINS- <i>fimT</i> <sub>Lp</sub> R143Q	pOPINS- <i>fimT</i> <sub>Lp</sub> , with <i>fimT</i> R143Q mutation	This study
pOPINS- <i>fimT</i> <sub>Lp</sub> R146Q	pOPINS- <i>fimT</i> <sub>Lp</sub> , with <i>fimT</i> R146Q mutation	This study
pOPINS- <i>fimT</i> <sub>Lp</sub> R148Q	pOPINS- <i>fimT</i> <sub>Lp</sub> , with <i>fimT</i> R148Q mutation	This study
pOPINS- <i>fimT</i> <sub>Lp</sub> R146Q, R148Q	pOPINS- <i>fimT</i> <sub>Lp</sub> , with <i>fimT</i> R146Q, R148Q mutations	This study
pOPINS- <i>fimT</i> <sub>Lp</sub> R143Q, R146Q, R148Q	pOPINS- <i>fimT</i> <sub>Lp</sub> , with <i>fimT</i> R143Q, R146Q, R148Q mutations	This study
pOPINS- <i>fimU</i> <sub>Lp</sub>	<i>L. pneumophila fimU</i> , residues 28-167	This study
pOPINS- <i>fimT</i> <sub>Pa</sub>	<i>Pseudomonas aeruginosa</i> PAO1 <i>fimT</i> (PA4549), residues 28-161	This study
pOPINS- <i>fimU</i> <sub>Pa</sub>	<i>P. aeruginosa</i> PAO1 <i>fimU</i> (PA4550), residues 28-159	This study

pOPINS- <i>fimT</i> <sub>Xc</sub>	<i>Xanthomonas campestris</i> ATCC 33913 <i>fimT</i> (XCC2486), residues 28-172	This study
pOPINS- <i>fimU</i> <sub>Xc</sub>	<i>X. campestris</i> ATCC 33913 <i>fimU</i> (XCC2495), residues 28-163	This study
pOPINB	<i>E. coli</i> expression vector: N-terminal His <sub>6</sub> -tag, T7 promoter; KanR	11
pOPINB- <i>pilA</i> 1 <sub>Lp</sub>	<i>L. pneumophila pilA1</i> ( <i>lpg1914</i> ), residues 25-132	This study
pOPINB- <i>pilA</i> 2 <sub>Lp</sub>	<i>L. pneumophila pilA2</i> , residues 25-131	This study
pTRC99A	<i>Ptc oriR</i> (pBR322); AmpR	12
pTRC99A- <i>lpg2953-2958::Kan</i>	<i>L. pneumophila</i> genomic region spanning <i>lpg2953-2958</i> . The <i>hipB</i> gene ( <i>lpg2955</i> ) is interrupted by kanamycin cassette, KanR	This study

1126

1127

1128

1129 **Extended Data Table 4: Oligonucleotides used in this study**

Name	Sequence (5' to 3')	Construct
<i>Cloning</i>		
pMMB207_lin_F	aattcgagctcggatcccg	pMMB207C
pMMB207_lin_R	ctgttcctgtgtgaaattgtatccgc	
fimT <sub>Lp</sub> _pMMB207C_F	tcacacaggaacagatgcggtcaattgatgaaaataacaggattt ac	pMMB207C- <i>fimT</i> <sub>Lp</sub>
fimT <sub>Lp</sub> _pMMB207C_R	taccgagctcgaattttaattaccccctaccctaaccctgccc	
fimT <sub>Lp</sub> R143Q_ pMMB207C_F	ccctaaccctgccaagctgatttaaagtaaccacaac	pMMB207C- <i>fimT</i> <sub>Lp</sub> R143Q
fimT <sub>Lp</sub> R143Q_ pMMB207C_R	ggttactttaatcagcttggcagggttagggtag	
fimT <sub>Lp</sub> R146Q_ pMMB207C_F	ctggccaggttagggtaggggtaattaaaattcg	pMMB207C- <i>fimT</i> <sub>Lp</sub> R146Q
fimT <sub>Lp</sub> R146Q_ pMMB207C_R	taccctaaccctggccaagcctatttaaagtaaccacaac	
fimT <sub>Lp</sub> R148Q_ pMMB207C_F	cagggttcaggttaggggtaattaaaattcgagctc	pMMB207C- <i>fimT</i> <sub>Lp</sub> R148Q
fimT <sub>Lp</sub> R148Q_ pMMB207C_R	cccctacctgaaccctgccaagcctatttaaag	
fimT <sub>Lp</sub> R146QR148Q_ pMMB207C_F	ctggccaggttcaggttaggggtaattaaaattcg	pMMB207C- <i>fimT</i> <sub>Lp</sub> R146Q, R148Q
fimT <sub>Lp</sub> R146QR148Q_ pMMB207C_R	cctacctgaaccctggccaagcctatttaaagtaac	
fimT <sub>Lp</sub> R143QR146QR148Q_ pMMB207C_F	gccaggttcaggttaggggtaattaaaattcgagctc	pMMB207C- <i>fimT</i> <sub>Lp</sub> R143Q, R146Q, R148Q
fimT <sub>Lp</sub> R143QR146QR148Q_ pMMB207C_R	ctacctgaaccctggccaagctgatttaaagtaaccacaacttttcattg	
pilA2 <sub>Lp</sub> -flag_ pMMB207C_F	tcacacaggaacagatggagatggcatgagacaaaagggttttac	pMMB207C- <i>pilA2</i> - flag
pilA2 <sub>Lp</sub> -flag_ pMMB207C_R	atcgtctttgtagtctgtctgcaactggcaggtc	
fimT <sub>Pa</sub> _pMMB207C_F	tcacacaggaacagatgggtcgaagggtcgcagagagc	pMMB207C- <i>fimT</i> <sub>Pa</sub>
fimT <sub>Pa</sub> _pMMB207C_R	taccgagctcgaatttcatccggaagtgtgcatagctc	
fimT <sub>Pa</sub> _125_pMMB207C_ F	ggtaaatttattttgtgcggaaggcattaccgtgc	pMMB207C- <i>fimT</i> <sub>chimera 1</sub>
fimT <sub>Lp</sub> _138_pMMB207C_ R	caaaataaattaccattactcatcgcacgattcg	
<i>fimT</i> <sub>Xc</sub> _pMMB207C_F	tcacacaggaacagatgagacaggacctcagtcacc	pMMB207C- <i>fimT</i> <sub>Xc</sub>
<i>fimT</i> <sub>Xc</sub> _pMMB207C_R	taccgagctcgaattttatgtctgagcaggtgccc	
<i>fimT</i> <sub>Xc</sub> _138_pMMB207C_ F	ggtaaatttattttgtgcattccagtcagagcaggtgg	pMMB207C- <i>fimT</i> <sub>chimera 2</sub>
fimT <sub>Lp</sub> _138_pMMB207C_ R	caaaataaattaccattactcatcgcacgattcg	
pSR47S_lin_F	ggatccccgggctgcaggaattcg	pSR47S
pSR47S_lin_R	ccactagtctagagcggccgccc	
fimT_HR_pSR47S_F	ggccgctctagaactagtgggtggcaaatgggatttaggtctccctcaatg	pSR47S- <i>fimT</i>
fimT_HR_pSR47S_R	cctgcagcccggggatccataaatgcctcagacaagctgacctctcc	
fimU_HR_pSR47S_F	ggccgctctagaactagtggccaacacatcactacctgttgagcattg c	pSR47S- <i>fimU</i>
fimU_HR_pSR47S_R	tcctgcagcccgggggatcccaatcactattgatgattgcctttgttggt g	
pilQ_HR_pSR47S_F	ggccgctctagaactagtgggtgaaaaaagcaacatcaggcagc	pSR47S- <i>pilQ</i>
pilQ_HR_pSR47S_R	tcctgcagcccgggggatccatcgaaacatcaacctcgccataaag	
pilT_HR_pSR47S_F	ggccgctctagaactagtgggtatcgtaatgagtgccaatattttcttacta atgc	pSR47S- <i>pilT</i>

pilT_HR_pSR47S_R	tcctgcagcccggggatccccgttacaataacacgtaattttaccaatt atgc	
comEC_HR_pSR47S_F	ggccgctctagaactagtggggtttaccacaacattatcactgccact g	pSR47S-comEC
comEC_HR_pSR47S_R	tcctgcagcccggggatccactctgcttgaaggtatcccagg	
ΔfimT_HR_pSR47S_F	tcttaaattataagcaatggtgttcataaagagg	pSR47S-ΔfimT
ΔfimT_HR_pSR47S_R	ccattgcttataatttaagacatctacaaaattttatgatgaagataagatg cg	
ΔfimU_HR_pSR47S_F	agcattatccctattgtttgatcgaaccac	pSR47S-ΔfimU
ΔfimU_HR_pSR47S_R	caaacaataggataatgctaacaacacccggccaagcagtc	
ΔpilQ_HR_pSR47S_F	tcaagattggactaattttatctcattaataaagataaaaaacattaattta atagc	pSR47S-ΔpilQ
ΔpilQ_HR_pSR47S_R	ttagtccaatcttgagcctcactcctgc	
ΔpilT_HR_pSR47S_F	atacacatgactgtgaaaaagacccaaggtc	pSR47S-ΔpilT
ΔpilT_HR_pSR47S_R	acaagtcattgttatactctataattcccgcc	
ΔcomEC_HR_pSR47S_F	atggattggctgacccatgttatatctaagc	pSR47S-ΔcomEC
ΔcomEC_HR_pSR47S_R	ggtcagccaatccattcaaatgaattggactttcc	
pOPINS_lin_F	taaagcttctagaccattaaacaccaccac	pOPINS
pOPINS_lin_R	accaccgatctgttcgcat	
fimT <sub>Lp</sub> _28_pOPINS_F	atcgcgaaacagatcggttggtatacaaaaataatgagagagaaacatta gttaatagataaaaaacagccattc	pOPINS-fimT <sub>Lp</sub>
fimT <sub>Lp</sub> _152_pOPINS_R	aaatggctagaaagctttattaattaccccctaccctaaccctgcc	
fimT <sub>Lp</sub> K103Q_pOPINS_F	tggaatattaattggcagggcgtagattcaaaccatag	pOPINS-fimT <sub>Lp</sub> K103Q
fimT <sub>Lp</sub> K103Q_pOPINS_R	tacgcctgccaattaatattccaggaattagaactcc	
fimT <sub>Lp</sub> R119Q_pOPINS_F	ccaatattccgaatcaggcgatgagtaatggtaaatttatttg	pOPINS-fimT <sub>Lp</sub> R119Q
fimT <sub>Lp</sub> R119Q_pOPINS_R	catcgctgattcggaatattggatataataattctatggtttgaatc	
fimT <sub>Lp</sub> R143Q_pOPINS_F	ggttactttaaatcagcttggcagggtagggtag	pOPINS-fimT <sub>Lp</sub> R143Q
fimT <sub>Lp</sub> R143Q_pOPINS_R	ccctaaccctgccaagctgatttaaagtaaccacaac	
fimT <sub>Lp</sub> R146Q_pOPINS_F	gcttggccaggttagggtaggggtaattaataaag	pOPINS-fimT <sub>Lp</sub> R146Q
fimT <sub>Lp</sub> R146Q_pOPINS_R	cctaacctggccaagcctatttaaagtaaccacaac	
fimT <sub>Lp</sub> R148Q_pOPINS_F	caggggtcaggttaggggtaattaataaagctttctagac	pOPINS-fimT <sub>Lp</sub> R148Q
fimT <sub>Lp</sub> R148Q_pOPINS_R	cccctacctgaaccctgccaagcctatttaaagtaac	
fimT <sub>Lp</sub> R146QR148Q_pOPINS_F	cttggccaggtcaggttaggggtaattaataaagc	pOPINS-fimT <sub>Lp</sub> R146Q, R148Q
fimT <sub>Lp</sub> R146QR148Q_pOPINS_R	ccctacctgaaccctggccaagcctatttaaagtaac	
fimT <sub>Lp</sub> R143QR146QR148Q_pOPINS_F	ggccaggttcaggttaggggtaattaataaagctttctag	pOPINS-fimT <sub>Lp</sub> R143Q, R146Q, R148Q
fimT <sub>Lp</sub> R143QR146QR148Q_pOPINS_R	tacctgaaccctggccaagctgatttaaagtaaccac	
fimU <sub>Lp</sub> _28_pOPINS_F	atcgcgaaacagatcggttggtattttgaatagccgttgactcaaacattg ac	pOPINS-fimU <sub>Lp</sub>
fimU <sub>Lp</sub> _167_pOPINS_R	atggtctagaaagctttattaagggcagttcaaagctccattattcc	
fimT <sub>Pa</sub> _28_pOPINS_F	atcgcgaaacagatcggttggtctggacggcaatcgcgagc	pOPINS-fimT <sub>Pa</sub>
fimT <sub>Pa</sub> _161_pOPINS_R	aaatggcttagaaagctttatcatccggaagtgtgcatagctc	
fimU <sub>Pa</sub> _28_pOPINS_F	atcgcgaaacagatcggttggtctgacagaacgcaacgaactgcag	pOPINS-fimU <sub>Pa</sub>
fimU <sub>Pa</sub> _159_pOPINS_R	aaatggcttagaaagctttatcaatagcatgactggggcgc	
fimT <sub>Xc</sub> _28_pOPINS_F	atcgcgaaacagatcggttggtatcgagcggcagcgggtg	pOPINS-fimT <sub>Xc</sub>
fimT <sub>Xc</sub> _172_pOPINS_R	aaatggcttagaaagctttattatgtctgagcaggtgcccgg	
fimU <sub>Xc</sub> _28_pOPINS_F	atcgcgaaacagatcggttggtattcggctgcaatcgcgctgttac	pOPINS-fimU <sub>Xc</sub>
fimU <sub>Xc</sub> _163_pOPINS_R	aaatggcttagaaagctttatcattgacagttatccttctactctgacttcg c	
pOPINB_lin_F	agcagcggctctggaagtctgtttcag	pOPINB
pOPINB_lin_R	atggtctagaaagcttta	
pilA1 <sub>Lp</sub> _25_pOPINB_F	aagttctgttcagggcccgaggactataccatcagagcac	pOPINB-pilA1 <sub>Lp</sub>
pilA1 <sub>Lp</sub> _132_pOPINB_R	atggtctagaaagctttattaagggcggcagtagg	

pilA2 <sub>Lp</sub> _28_pOPINB_F	aagttctgttcagggcccgaagattacacaatacgagctcg	pOPINB-pilA2 <sub>Lp</sub>
pilA2 <sub>Lp</sub> _131_pOPINB_R	atggctagaaagctttattatggctgcaactggcag	
pTRC99A_lin_F	gtgtctagagtcgacctgcaggcat	pTRC99A
pTRC99A_lin_R	gaacacaccagagatatctggcagaattc	
Lpg2953_F	atctctggtgtgttcggatagattatgagagaggtctattgaagattctctg actatg	pTRC99A-lpg2953- 2958::Kan Amplification of transforming DNA
Lpg2958_R	gtcgactctagacacagacatggcctggaaacggttggtggg	
KanR_lin_F	cattcaaataatgatccgctcatga	pTRC99A-lpg2953- 2958::Kan
KanR_lin_R	cggggctcgacgctcagt	
pTRC99A_lpg2953_F	atacatattgaatgcacgaatttctattctttggcc	pTRC99A-lpg2953- 2958::Kan
pTRC99A_lpg2958_R	gagcgtcagaccccggtttggcagttttctcttca	
<i>DNA-binding assays*</i>		
FAM-12mer	# gttcgcaacgaa	MST/TRIC
12mer	gttcgcaacgaa	NMR titrations/ITC
FAM-30mer	# ttaaataggcttggcagggttaggtaggg	EMSA
30mer	ttaaataggcttggcagggttaggtaggg	EMSA

1130 \* The complementary strand for dsDNA probes is not shown. Only one of the two strands is  
1131 fluorescein (FAM)-labelled.

1132 # Indicates the position of the FAM label.

1133



1134  
1135  
1136

**Extended Data Table 5:** Gene locus tags of *fimT* and *fimU* genes from previous and recently updated genomes

	<i>L. pneumophila</i> Philadelphia 1 (old)*	<i>L. pneumophila</i> Philadelphia 1 (new)	<i>X. campestris</i> ATCC 33913 (old)*	<i>X. campestris</i> ATCC 33913 (new)	<i>A. baylyi</i> ADP1 (old)	<i>A. baylyi</i> ADP1 (new)
<b>RefSeq</b>	NC_002942.5	NC_002942	NC_003902.1	NC_003902	NC_005966.1	NC_005966
<b>Release date</b>	2014	2021	2014	2021	2015	2020
<i>fimT</i>	<i>lpg1428</i>	LPG_RS07155	XCC2486	XCC_RS12930	ACIAD0695	ACIAD_RS03200
<i>fimU</i>	<i>lpg0632</i>	LPG_RS03130	XCC2495	XCC_RS12975	ACIAD3321	ACIAD_RS15030

1137  
1138  
1139  
1140  
1141  
1142  
1143

\* In this study we have referred to the old locus tags throughout.

**Extended Data Table 6:** Gene locus tags of selected genes from this study from previous and recently updated genomes

	<i>L. pneumophila</i> Philadelphia 1 (old)*	<i>L. pneumophila</i> Philadelphia 1 (new)
<b>RefSeq</b>	NC_002942.5	NC_002942
<b>Release date</b>	2014	2021
<i>pilQ</i>	<i>lpg0931</i>	LPG_RS04620
<i>pilT</i>	<i>lpg2013</i>	LPG_RS10105
<i>comEC</i>	<i>lpg0626</i>	LPG_RS03100
<i>pilA1</i>	<i>lpg1914</i>	LPG_RS09600
<i>pilA2</i>	<i>lpg1915</i>	LPG_RS09605
<i>hipB</i>	<i>lpg2955</i>	LPG_RS14950
<i>pilV</i>	<i>lpg0631</i>	LPG_RS03125
<i>pilW</i>	<i>lpg0630</i>	LPG_RS03120
<i>pilX</i>	<i>lpg0629</i>	LPG_RS03115
<i>pilY1</i>	<i>lpg0628</i>	LPG_RS03110
<i>pilE</i>	<i>lpg0627</i>	LPG_RS03105

1144  
1145

\* In this study we have referred to the old locus tags throughout.

1146 **References**

1147

1148 1. Yanez, M. E., Korotkov, K. K., Abendroth, J. & Hol, W. G. J. Structure of the Minor Pseudopilin  
1149 EpsH from the Type 2 Secretion System of *Vibrio cholerae*. *Journal of Molecular Biology* **377**, 91–103  
1150 (2008).

1151 2. Landau, M. *et al.* ConSurf 2005: the projection of evolutionary conservation scores of residues on  
1152 protein structures. *Nucleic Acids Res* **33**, W299–W302 (2005).

1153 3. Berry, J.-L. *et al.* A Comparative Structure/Function Analysis of Two Type IV Pilin DNA Receptors  
1154 Defines a Novel Mode of DNA Binding. *Structure* **24**, 926–934 (2016).

1155 4. Zuckman, D. M., Hung, J. B. & Roy, C. R. Pore-forming activity is not sufficient for *Legionella*  
1156 *pneumophila* phagosome trafficking and intracellular growth. *Molecular microbiology* **32**, 990–1001  
1157 (1999).

1158 5. Kolter, R., M, I. & R, H. D. Trans-Complementation-Dependent Replication of a Low Molecular  
1159 Weight Origin Fragment from Plasmid R6K. *Cell* **15**, 1199–1208 (1978).

1160 6. Finan, T. M., Kunkel, B., Vos, G. F. D. & Signer, E. R. Second Symbiotic Megaplasmid in  
1161 *Rhizobium meliloti* Carrying Exopolysaccharide and Thiamine Synthesis Genes. *Journal of*  
1162 *bacteriology* **167**, 66–72 (1986).

1163 7. Berger, K. H. & Isberg, R. R. Two distinct defects in intracellular growth complemented by a single  
1164 genetic locus in *Legionella pneumophila*. *Molecular microbiology* **7**, 7–19 (1993).

1165 8. Chen, J. *et al.* *Legionella* Effectors That Promote Nonlytic Release from Protozoa. *Science* **303**,  
1166 1358–1361 (2004).

1167 9. Merriam, J. J., Mathur, R., Maxfield-Boumil, R. & Isberg, R. R. Analysis of the *Legionella*  
1168 *pneumophila* flil Gene: Intracellular Growth of a Defined Mutant Defective for Flagellum Biosynthesis.  
1169 *Infection and immunity* **65**, 2497–2501 (1997).

1170 10. Assenberg, R. *et al.* Expression, purification and crystallization of a lyssavirus matrix (M) protein.  
1171 *Acta Crystallogr Sect F Struct Biology Cryst Commun* **64**, 258–262 (2008).

1172 11. Berrow, N. S. *et al.* A versatile ligation-independent cloning method suitable for high-throughput  
1173 expression screening applications. *Nucleic Acids Research* **35**, e45–e45 (2007).

1174 12. Amann, E., Ochs, B. & Abel, K.-J. Tightly regulated tac promoter vectors useful for the expression  
1175 of unfused and fused proteins in *Escherichia coli*. *Gene* **69**, 301–315 (1988).

1176

1177

1178